

A control-oriented approach to estimate the injected fuel mass on the basis of the measured in-cylinder pressure in multiple injection diesel engines

Original

A control-oriented approach to estimate the injected fuel mass on the basis of the measured in-cylinder pressure in multiple injection diesel engines / Finesso, Roberto; Spessa, Ezio. - In: ENERGY CONVERSION AND MANAGEMENT. - ISSN 0196-8904. - STAMPA. - 105:(2015), pp. 54-70. [10.1016/j.enconman.2015.07.053]

Availability:

This version is available at: 11583/2615746 since: 2021-03-25T17:40:00Z

Publisher:

Elsevier

Published

DOI:10.1016/j.enconman.2015.07.053

Terms of use:

This article is made available under terms and conditions as specified in the corresponding bibliographic description in the repository

Publisher copyright

(Article begins on next page)

**A CONTROL-ORIENTED APPROACH TO ESTIMATE THE INJECTED FUEL MASS
ON THE BASIS OF THE MEASURED IN-CYLINDER PRESSURE IN MULTIPLE
INJECTION DIESEL ENGINES**

*Roberto Finesso, Ezio Spessa**

IC Engines Advanced Laboratory, Politecnico di Torino

c.so Duca degli Abruzzi 24, 10129 - Torino, Italy

Key Words: diesel, control-oriented, injection, pilot, main

ABSTRACT

A new control-oriented methodology has been developed to estimate the injected fuel quantities, in real-time, in multiple injection DI diesel engines on the basis of the measured in-cylinder pressure.

The method is based on the inversion of a predictive combustion model that was previously developed by the authors, and that is capable of estimating the heat release rate and the in-cylinder pressure on the basis of the injection rate. The model equations have been rewritten in order to derive the injected mass as an output quantity, starting from use of the measured in-cylinder pressure as input.

It has been verified that the proposed method is capable of estimating the injected mass of pilot pulses with an uncertainty of the order of ± 0.15 mg/cyc, and the total injected mass with an uncertainty of the order of ± 0.9 mg/cyc. The main sources of uncertainty are related to the estimation of the in-cylinder heat transfer and of the isentropic coefficient $\gamma = c_p/c_v$.

The estimation of the actual injected quantities in the combustion chamber can represent a

*Corresponding Author: Tel. +39-011.090.4482; Fax: +39-011.090.4599; e-mail: ezio.spessa@polito.it

25 powerful means to diagnose the behavior of the injectors during engine operation, and offers
26 the possibility of monitoring effects, such as injector ageing and injector coking, as well as of
27 allowing an accurate control of the pilot injected quantities to be obtained; the latter are in fact
28 usually characterized by a large dispersion, with negative consequences on the combustion
29 quality and emission formation.

30 The approach is characterized by a very low computational time, and is therefore suitable
31 for control-oriented applications.

32

33 **NOMENCLATURE**

34 *A*: heat transfer area

35 *AC*: Alternating Current

36 *B*: Bore diameter

37 *BDC*: Bottom Dead Center

38 *BMEP*: Brake Mean Effective Pressure

39 *BTDC*: Before Top Dead Center

40 *c*: coefficient of sensitivity

41 *CA*: crank angle

42 *c₀*: Woschni heat transfer calibration coefficient

43 *CLD*: Chemi-Luminescence Detector

44 *c_p*: specific heat at constant pressure

45 *c_v*: specific heat at constant volume

46 *DI*: Direct Injection

47 *DoE*: Design of Experiment

48 *DT*: Dwell Time

49 *ECU*: Electronic Control Unit

50	<i>EGR</i> : Exhaust Gas Recirculation
51	<i>EOC</i> : End of Combustion
52	<i>EOI</i> : End of Injection
53	<i>ET</i> : Energizing Time
54	<i>EVO</i> : Exhaust Valve Opening
55	<i>GMPT-E</i> : General Motors PowerTrain-Europe
56	<i>h</i> : heat transfer convective coefficient
57	<i>H_L</i> : lower heating value of the fuel
58	<i>HLM</i> : HRR local minima criterion to estimate the SOC of intermediate pulses
59	<i>HRR</i> : Heat Release Rate
60	<i>ICEAL-PT</i> : Internal Combustion Engine Advanced Laboratory at the Politecnico di Torino
61	<i>IMEP</i> : Indicated Mean Effective Pressure
62	<i>IVC</i> : Intake Valve Closing
63	<i>k</i> : coverage factor
64	<i>K</i> : combustion rate parameter of the heat release model
65	<i>m</i> : compression phase polytropic coefficient; mass
66	$\dot{m}_{f, inj}$: fuel injection rate
67	<i>MFB50</i> : crank angle at which 50% of the fuel mass fraction has burned
68	<i>n</i> : engine speed
69	<i>NEDC</i> : New European Driving Cycle
70	<i>p</i> : pressure
71	<i>PCCI</i> : Premixed Charge Compression Ignition
72	<i>p_f</i> : injection pressure
73	<i>PPF</i> : Peak Firing Pressure

- 74 p_{int} : intake manifold pressure
- 75 p_m : motored pressure
- 76 q : generic injected fuel quantity [mm³]
- 77 $q_{f,inj}$: total injected fuel quantity [mm³]
- 78 $q_{pil,tot}$: total injected fuel quantity of the pilot pulses [mm³]
- 79 Q : energy
- 80 Q_{ch} : released chemical energy
- 81 Q_{fuel} : chemical energy of the injected fuel
- 82 Q_{ht} : heat exchanged by the charge with the walls
- 83 $Q_{ht, glob}$: heat globally exchanged by the charge with the walls over the combustion period
- 84 Q_{net} : net energy
- 85 R : gas constant
- 86 R^2 : squared correlation coefficient
- 87 $RAFR$: relative air-to-fuel ratio
- 88 $RMSE$: root mean square of the error
- 89 SOC : Start of Combustion
- 90 SOI : Start of Injection
- 91 S_p : Mean piston speed
- 92 t : time
- 93 T : temperature
- 94 TAF : time average filtering
- 95 T_{int} : intake manifold temperature
- 96 T_{sor} : temperature evaluated at SOI
- 97 T_w : wall temperature
- 98 TDC : Top Dead Center

99	u^2 : variance
100	U : Expanded uncertainty
101	V : volume
102	V_d : cylinder displacement
103	WG : wastegate
104	<i>Greek Symbols</i>
105	$\gamma = c_p/c_v$: isentropic coefficient
106	ρ : density
107	ρ_{sor} : density evaluated at SOI
108	τ : ignition delay parameter of the heat release model
109	
110	<i>Subscripts</i>
111	exp : experimental
112	f, inj : injected fuel
113	$f, evap$: evaporated fuel
114	$glob$: global
115	ht : heat transfer
116	inj : injected
117	int : related to the intake manifold
118	$main$: related to the main injection
119	pil : related to the pilot injection
120	
121	<i>Superscripts</i>
122	SOC : calculated from the start of combustion

123

124 *Notation*

125 *: constant in time

126

127 1. INTRODUCTION

128 Modern DI diesel engines usually adopt multiple injections in order to optimize pollutant
129 formation, combustion noise and efficiency [1-3]. The injected fuel quantity of each pulse is
130 usually set by the ECU (Electronic Control Unit) in open-loop control mode, on the basis of an
131 injector map; this map usually provides the injected quantity as a function of the energizing time
132 (ET) (i.e., the duration of the electric command provided to the injector) and of the injection
133 pressure (p_f), and is derived from an experimental steady-state characterization of the injectors
134 performed at the hydraulic test bench [4, 5]. However, a real-time control of the actual injected
135 quantities has not yet been developed. The actual quantity of fuel that is injected into the
136 combustion chamber can in fact be very different from that resulting from the steady-state
137 injector map, as a consequence of several effects. First, the dynamic pressure effects that are
138 induced in the pipes by multiple injection strategies may lead to a variability of the actual
139 injected quantities even for a constant ET, depending on the time interval between consecutive
140 injections (i.e., on the dwell-time DT) and on the injection pressure [4, 5]. Moreover, effects
141 such as injector ageing and coking [6] may lead to a worsening of the injection system
142 performance, which cannot currently be predicted by ECUs.

143 A critical situation occurs for pilot injections, in which the injected quantity is very small.
144 The actual amount of injected fuel mass of the pilot pulses may in fact be highly dispersed
145 during engine operation, and this may depend on the injection parameters (i.e., DT, p_f) or on
146 injection system ageing. Considering that pilot pulses affect pollutant formation [2, 7], and
147 above all soot formation [8] to a great extent, it could be very useful to be able to perform

148 real-time diagnostics of the actual injected fuel mass in the combustion chamber during engine
149 operation in order to improve the combustion quality and to reduce engine-out pollutant
150 emissions.

151 Interest in control-oriented predictive combustion models that simulate the heat release rate and
152 in-cylinder pressure in diesel engines has been growing over the last few years, due to their good
153 predictive capability and the increasing computational performance of modern ECUs [9-17]. One of
154 the most widely adopted methods used to simulate the heat release in DI diesel engines is the
155 accumulated fuel mass approach [11-17]. This method is based on the assumption that the rate of
156 released chemical energy is proportional to the energy associated with the fuel quantity made
157 available for combustion at the considered instant. This energy can be computed at time t as the
158 difference between the chemical energy associated with the injected fuel quantity and the
159 cumulative heat release. The accumulated fuel mass method has the great advantage of being able to
160 directly relate the injection rate to the combustion rate, and is therefore physically consistent. This
161 approach has been applied extensively and successfully to a wide range of engine hardware setups
162 and operating conditions [13-17].

163 The capability of this model to correctly correlate the injection rate with the heat release rate has
164 suggested the possibility of using the same model to derive the injected fuel mass as an output
165 quantity, starting from the experimental heat release rate that is obtained from the measured
166 in-cylinder pressure. The model equations have therefore been rewritten in order to derive the
167 injected fuel mass as a function of the heat release rate. The proposed methodology therefore
168 requires the measurement of the in-cylinder pressure, which can be carried out by means of pressure
169 sensors embedded in the glow-plugs (e.g., see [18]); these pressure sensors could also be used for
170 closed-loop combustion control tasks as shown in [18].

171 The investigation has been carried out on a GM 2.0 L diesel engine at several representative
172 key-points of the NEDC (New European Driving Cycle), which feature a pilot-main injection

173 strategy. The approach that is proposed in this study to estimate the actual injected quantities is
174 based on combustion diagnostics; alternative methods based on the measurement of hydraulic
175 variables in the injection system, have already been proposed in the literature, such as those
176 reported in [19-20]. In that study, a miniaturized hot-film anemometer with titanium/platinum
177 metallization was developed on a low-temperature co-fired ceramics substrate and integrated in
178 a Common Rail injection nozzle, so that the injected fluid velocity could be measured. The
179 integration of a ceramic flow sensor chip in the nozzle leads to an additional cost compared to
180 the baseline injector configuration. Moreover, it may cause some disturbances to the fluid
181 properties inside the nozzle and induce a reduction in the injected quantities. However, it offers
182 the advantage of being able to directly monitor the injected fuel velocity in each injector.

183 The method proposed in the present study is based on the measured in-cylinder pressure. This
184 solution also requires an additional cost, related to the need to install integrated pressure sensors
185 in the cylinders; however, these sensors can also be used for additional tasks, such as
186 closed-loop combustion control of combustion phasing. An advantage of the proposed method is
187 that it does not cause disturbances in the fluid properties inside the nozzle; however, a limit in
188 the minimum dwell-time between consecutive injections is introduced, as the method assumes
189 that any heat release overlapping between consecutive injection pulses is negligible.

190 In the present investigation, a comparison was made between the injected quantities that are
191 predicted by the model and those which are derived from the ECU on the basis of the injector
192 map. The total injected quantity predicted by the model was also compared with that derived
193 from a fuel flow meter. The investigation was carried out on some representative operating
194 conditions of the NEDC.

195 A sensitivity analysis on the effects of the main model parameters was also carried out, and
196 the uncertainty of the estimated injected quantities was evaluated.

197 Finally, an analysis of the required computational time was also done.

198

199 2. TEST ENGINE AND EXPERIMENTAL SETUP

200 The model has been assessed and applied to a Euro 5 GMPT-E 2.0 L engine equipped with a
 201 twin-stage turbocharger and with piezo-driven injectors. The main engine specifications are
 202 reported in Table 1.

203 **Table 1 – Main specifications of the Euro 5 diesel engine.**

Engine type	2.0L “Twin-Stage” Euro 5
Displacement	1956 cm ³
Bore x stroke	83.0 mm x 90.4 mm
Connecting rod length	145 mm
Compression ratio	16.5
Valves per cylinder	4
Turbocharger	Twin-stage with valve actuators and WG
Fuel injection system	Common Rail 2000 bar piezo
Specific power and torque	71 kW/l – 205 Nm/l
Injector specifications	d=137 μm, C _d = 0.8, C _a =0.84, C _v =0.95

204

205 The experimental data were acquired in a previous research activity that was financially
 206 supported by GMPT-E and which had the aim of investigating the potentialities of innovative piezo-
 207 and solenoid-driven Common Rail injection systems on engine performance, emissions, fuel
 208 consumption and combustion [3]. The experimental tests, related to the engine and to the injectors,
 209 were carried out at the highly dynamic test bed and at the hydraulic test rig at ICEAL-PT (Internal
 210 Combustion Engine Advanced Laboratory at the Politecnico di Torino).

211 The experimental characterization of the injectors was carried out at the Bosch-Moehwald
 212 hydraulic bench [4-5], which is instrumented for a complete fluid-dynamic characterization of
 213 Common Rail fuel-injection systems, and includes an EVI injection-rate meter, an EMI2 device to
 214 gauge the oil injected mass as well as thermo-piezo-transducers to measure temperature and

215 pressure traces in the rail and at the injector inlet.

216 The engine dynamic test rig was equipped with: an ‘ELIN AVL APA 100’ cradle-mounted AC
217 dynamometer, featuring a power of 220 kW, a nominal torque of 525 Nm, and a maximum speed of
218 12000 rpm; an ‘AVL KMA 4000’ system, used to continuously meter engine fuel consumption;
219 an ‘AVL AMAi60’ raw exhaust-gas analyzer.

220 All of the abovementioned measuring instruments were controlled by the AVL PUMA
221 OPEN 1.3.2 automation system. The test bed environment was interfaced with AVL CAMEO
222 software to run intelligent engine calibration procedures on the basis of the DoE (Design of
223 Experiment) approach.

224 The engine was fully instrumented with piezoresistive pressure transducers and K and T
225 thermocouples to measure the pressure and temperature levels at various engine locations. An
226 ‘NGK’ UEGO air-fuel ratio sensor was placed inside the exhaust system. A Kistler 6058A41
227 high-frequency piezoelectric transducer was fitted to the glow-plug seat to measure the
228 in-cylinder pressure time-histories. The in-chamber pressure traces were referenced on the
229 basis of the pressure in the intake manifold, which was measured by means of a high-frequency
230 Kistler 4075A10 piezoresistive transducer. The latter was located at the inlet runner of the
231 cylinder equipped with the in-cylinder pressure sensor.

232

233 *2.1. Experimental tests*

234 The method was tested on six key-points (expressed in terms of engine speed x BMEP),
235 which were identified in order to characterize the engine operations in a medium-sized
236 passenger car over an NEDC. The key-points are: 1500x2, 1500x5, 2000x2, 2000x5, 2500x8,
237 2750x12 rpm x bar. Table 2 summarizes the main engine parameters for the six analyzed tests.

238 **Table 2 – Main specifications of the six analyzed key-points.**

Key-point	p_r	Intake O ₂	p_{int}	q_{pil} (ECU)	$q_{f,inj}$ (ECU)	SOI pil	SOI main
	bar	%	bar	mm ³	mm ³	deg BTDC	deg BTDC
1500x2	458	15.98	0.963	1.7	7.6	10.7	-2.37
1500x5	589	16.73	1.169	1.6	17.3	12.2	-0.75
2000x2	554	16.58	1.051	1.6	9.3	16.2	-0.86
2000x5	753	16.73	1.373	1.4	18.2	17.0	-0.12
2500x8	1198	17.83	2.01	1.2	33.2	25.4	3.84
2750x12	1481	17.69	2.23	1.1	46.7	30.5	6.63

3. DESCRIPTION OF THE COMBUSTION MODEL

A detailed description of the model, including the calibration and validation procedures, has already been given in detail in [13-15]. However, a summary is reported hereafter for the sake of clarity.

The heat release model is based on the accumulated fuel mass approach, which assumes that, at any time instant, the rate of chemical energy released by the fuel is proportional to the energy associated with the in-cylinder accumulated fuel mass. This energy can be calculated at time instant t as the difference between the chemical energy of the injected fuel mass and the released chemical energy.

The released chemical energy $Q_{ch,j}$ at time t , for each pulse j ($1 \leq j \leq N$) of the injection event, is therefore evaluated as follows:

$$\frac{dQ_{ch,j}}{dt} = K_j \left[Q_{fuel,j}(t - \tau_j) - Q_{ch,j}(t) \right] \quad (1)$$

where K_j and τ_j are model calibration quantities, related to the combustion rate and to the ignition delay, respectively, and $Q_{fuel,j}$ is the chemical energy associated with the injected fuel mass:

$$Q_{fuel,j} = \int_{t_{SOI,j}}^t \dot{m}_{f,inj} H_L dt \quad t \leq t_{EOI,j} \quad (2)$$

$$Q_{fuel,j} = \int_{t_{SOI,j}}^{t_{EOI,j}} \dot{m}_{f,inj} H_L dt \quad t > t_{EOI,j} \quad (3)$$

SOI and EOI denote the start and end of injection, respectively, $\dot{m}_{f,inj}$ the injection rate and H_L the lower heating value of the fuel. The total released chemical energy can be calculated as the sum of the contributions of all the injection pulses:

$$Q_{ch} = \sum_{j=1}^N Q_{ch,j} \quad (4)$$

The K_j and τ_j parameters have to be appropriately tuned in order to obtain a good matching between the predicted Q_{ch} curves and those derived from the experimental in-cylinder pressure [13].

The calibration is performed for several steady-state operating conditions, and physically-consistent correlations are then derived as a function of significant engine variables. The tuning procedure of the model for the engine considered in this study is reported in [15].

With reference to the combustion rate coefficients, it was found, in [13-15], that a constant value can be taken for the combustion rate parameter of the pilot pulse (i.e., K_{pil}). Instead, it was shown, in [13-15], that a dependence exists between the combustion rate parameter of the main pulse (i.e., K_{main}) and the engine speed/load conditions, and this dependence can be taken into account either by means of a look-up table or by means of simple correlations such as those shown in [13]. In addition, a reduction factor was introduced in [15] to correctly account for low-density/low-oxygen operating conditions, which may induce a remarkable decrease in the combustion rate.

The ignition delay parameters were studied in detail in [21], and the following correlations were identified for the engine considered in the present study:

$$\tau_{pil} = 0.008977 \rho_{SOI}^2 - 0.36077 \rho_{SOI} + 3.8619 \quad (5)$$

$$\tau_{main} = 3.8E4 \rho_{SOI}^{-2.2} \exp\left(\frac{2100}{T_{SOI}}\right) O_2^{-1.9} p_f^{-0.31} q_{pil,tot}^{-0.35} \quad (6)$$

Equation (5) indicates that only the charge density calculated at SOI (ρ_{SOI}) is necessary for

280 a good estimation of the ignition delay of the pilot injections, as the physical contribution is
 281 predominant over the chemical one [21]. Instead, the effect of the intake charge oxygen
 282 concentration (O_2), of the charge density and temperature at SOI (ρ_{SOI} , T_{SOI}), of the injection
 283 pressure (p_f) and of the total injected pilot quantity ($q_{pil,tot}$) have to be included to accurately predict
 284 the ignition delay of the main pulse.

285 ρ_{SOI} and T_{SOI} are calculated assuming that the in-chamber thermodynamic conditions at BDC
 286 are equal to those in the intake manifold (p_{int} , T_{int}):

$$287 \quad \rho_{SOI} = \frac{P_{int}}{RT_{int}} \left(\frac{V_{BDC}}{V_{SOI}} \right) \quad (7)$$

$$288 \quad T_{SOI} = T_{int} \left(\frac{V_{BDC}}{V_{SOI}} \right)^{m-1} \quad (8)$$

289 where m is the polytropic coefficient during the compression phase.

290 The choice of using BDC as the reference angle to estimate ρ_{SOI} and T_{SOI} is just a convention.
 291 It was in fact verified that the values of ρ_{SOI} and T_{SOI} obtained using, for example, IVC as the
 292 reference crank angle are very similar (i.e., the root mean square difference is of the order of 0.34
 293 kg/m³ and 5.3 K, respectively, for the key-points analyzed in the present paper).

294 The values of ρ_{SOI} and T_{SOI} obtained using Eq. (7) and Eq. (8) are obviously approximations of
 295 the actual values inside the combustion chamber. The actual values of ρ_{SOI} could be estimated by
 296 dividing the total trapped mass by the in-chamber volume at SOI. The total trapped mass is the sum
 297 of the trapped air mass, of the trapped EGR mass and of the residual gas mass. The different
 298 contributions could be evaluated on the basis of the air-to-fuel ratio and of the EGR rate, which can
 299 in turn be estimated with the procedure shown in [22]. The actual T_{SOI} values could instead be
 300 evaluated by applying the ideal gas law at SOI, using the values of the in-cylinder pressure at SOI
 301 and of the total trapped mass.

Figure 1a shows a comparison between the actual values of ρ_{SOI} and those obtained using Eq. (7), while Fig. 1b shows a comparison between the actual values of T_{SOI} and those obtained using Eq. (8), for the key-points analyzed in the present study.

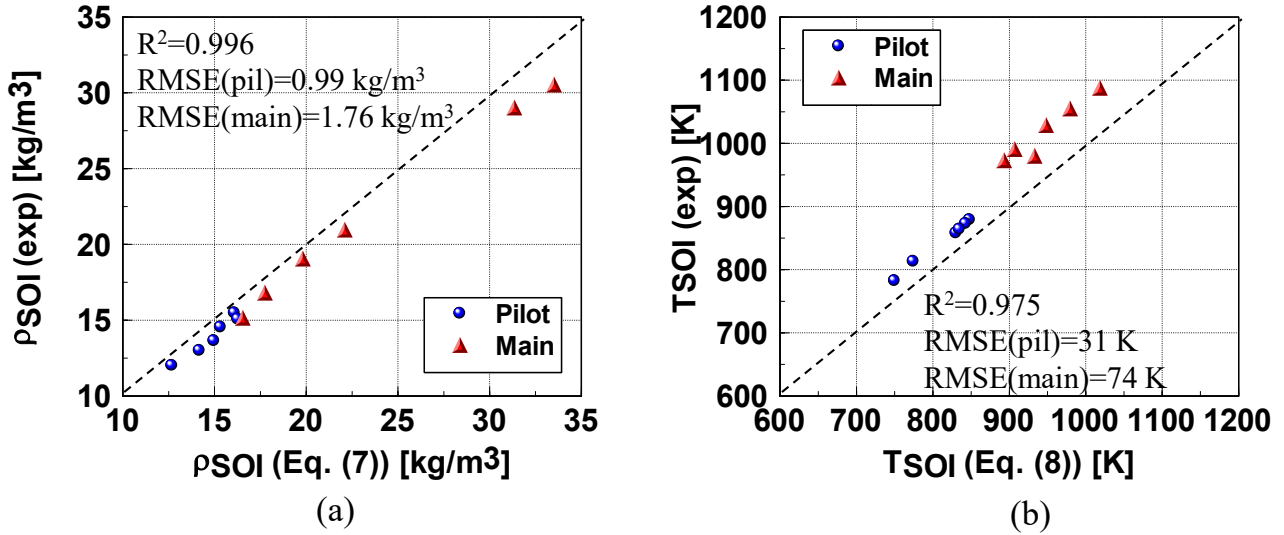


Figure 1 – Experimental vs. calculated values of ρ_{SOI} using Eq. (7) (a); experimental vs. calculated values of T_{SOI} using Eq. (8) (b).

In general, the approximation of the density is quite good, as the average root mean square (RMS) difference is 0.99 kg/m^3 for the $\rho_{SOI,pil}$ term and 1.76 kg/m^3 for the $\rho_{SOI,main}$ term (the use of Eq. (7) leads to an overestimation). With reference to T_{SOI} , it can be seen that the average root mean square difference between the values obtained with Eq. (8) and the actual ones are 31 K for $T_{SOI,pil}$ and 74 K for $T_{SOI,main}$. The underestimation obtained using Eq. (8) is mainly due to the heat transfer effects during the intake phase and to the residual gas contribution being neglected. Moreover, the greater overestimation of $T_{SOI,main}$ is due to the charge heating caused by the pilot combustion being neglected.

However, it can be seen, in Fig. 1, that the use of Eqs. (7-8) allows the trends of ρ_{SOI} and T_{SOI} to be captured, so that the differences, with respect to the true values, are indirectly taken into account through the tuning of the exponents in Eqs. (5-6). Moreover, Eqs. (7-8) require the intake manifold pressure and temperature, which are known quantities for the ECU, as input,

320 and they can therefore be considered suitable for control-oriented applications.

321 O_2 can be derived from the real-time EGR and intake charge model [23], while p_f and
322 $q_{pil,tot}$ are known quantities for the engine ECU.

323 The predicted released chemical energy Q_{ch} can be used as a starting quantity to evaluate the
324 charge net energy (i.e., Q_{net}) which is given, at each time instant, by the difference between the
325 released chemical energy and the heat exchanged by the charge with the walls, i.e., Q_{ht} [24]:

326
$$Q_{net} = Q_{ch} - Q_{ht} \quad (9)$$

327 Q_{net} can be approximated by means of a uniform scaling of the Q_{ch} curve, according to the
328 procedure proposed in [13-15]; the scaling factor includes the global heat exchanged between the
329 charge and the walls over the combustion period, i.e., $Q_{ht,glob}$.

330 The net energy of the charge can therefore be approximated as follows [13]:

331
$$Q_{net}^{SOC} \cong Q_{ch} \frac{m_{f,inj}^* H_L - Q_{ht,glob}}{m_{f,inj}^* H_L} \quad (10)$$

332 where $m_{f,inj}^*$ is the total injected fuel mass and H_L the lower heating value of the fuel; the
333 superscript (SOC) indicates that Q_{net} is evaluated from the start of combustion onwards. The $Q_{ht,glob}$
334 parameter must be known in order to apply Eq. (10). In general, it is necessary to derive a
335 physically consistent correlation for this parameter, such as that proposed in [13], as a function of
336 the ratio between the injected fuel quantity and the engine speed. The experimental values of $Q_{ht,glob}$,
337 which are necessary to identify this correlation, are calculated as the difference between the
338 chemical energy of the total injected mass (i.e., $m_{f,inj}^* H_L$) and the value of the experimental net
339 energy curve evaluated at the end of combustion. The experimental net energy curve ($Q_{net,exp}^{SOC}$) can
340 be derived from the measured in-cylinder pressure using a single zone approach [24]:

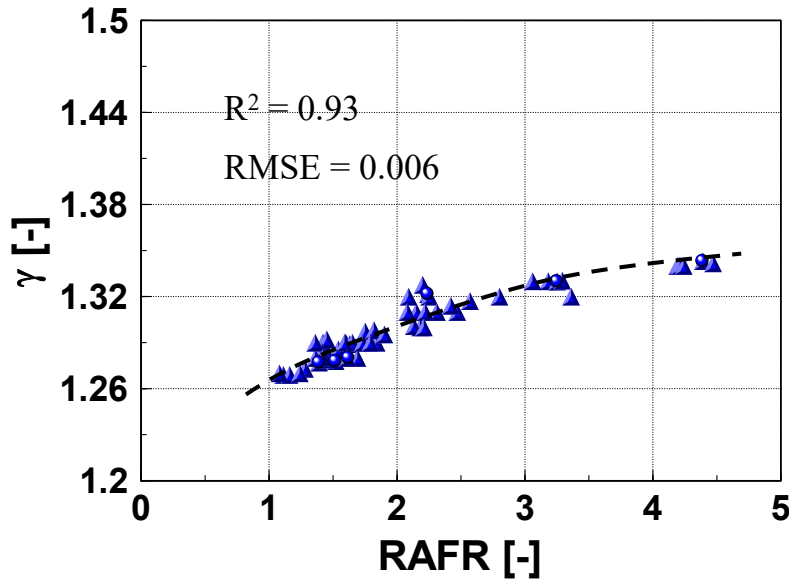
341
$$dQ_{net,exp}^{SOC} = \frac{\gamma}{\gamma - 1} p_{exp} dV + \frac{1}{\gamma - 1} V dp_{exp} \quad (t \geq t_{SOC}) \quad (11)$$

342 where $\gamma = \frac{c_p}{c_v}$ is the ratio of the specific heats, and was evaluated as a function of the

343 relative air-to-fuel ratio, according to the correlation that was proposed in [13]:

344
$$\gamma = -0.0064RAFR^2 + 0.0563RAFR + 1.2151 \quad (12)$$

345 The experimental values of γ used to derive Eq. (12) are shown in Fig. 2, and were derived
 346 in [13] for a 1.9L GM diesel engine using different values of the compression ratio. The values of
 347 the squared correlation coefficient R^2 and of the root mean square error (RMSE) for the
 348 predicted vs. experimental values of γ are also reported in the chart.



349
 350 **Figure 2– Trend of the experimental values of the γ parameter as a function of the**
 351 **relative air-to-fuel ratio [13].**

352 The experimental value of $Q_{ht, glob}$ is therefore calculated as follows:

353
$$Q_{ht, glob, exp} = m_{f, inj}^* H_L - Q_{net, exp}^{SOC}(t_{EOC}) \quad (13)$$

354 It is convenient to use an accurate estimate of the total injected mass in Eq. (13) (e.g., that
 355 derived from a fuel flow meter) in order to accurately evaluate the global heat transfer parameter.
 356 The calibration of the $Q_{ht, glob}$ parameter was carried out in [13-15] using the values of the fuel
 357 flow rate that were measured by means of a fuel flow meter installed at the test bed; this flow rate

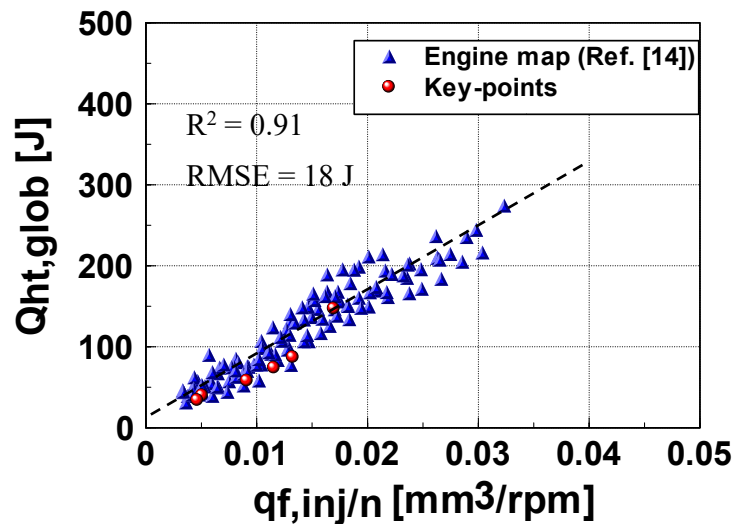
358 was split into equal parts over the 4 cylinders, and converted into an average injected mass per cycle.
 359 It has in fact been verified that, for the present engine, the performance of the four injectors is similar
 360 (see section 3.1).

361 It was found in [13-15] that $Q_{ht, glob}$ is well correlated with the $q_{f, inj}/n$ parameter, where $q_{f, inj}$
 362 indicates the total injected quantity of fuel and n the engine speed. The following correlation was
 363 derived from engine map tests acquired on a GM 1.9L diesel engine with a similar hardware setup to
 364 that of the present study, but equipped with solenoidal injectors (see [14]):

$$365 \quad Q_{ht, glob} = 7656 \cdot \frac{q_{f, inj} [mm^3]}{n [rpm]} + 14.4 \text{ J} \quad (14)$$

366 Figure 3 shows the experimentally-derived values of $Q_{ht, glob}$ that were used to identify Eq. (14)
 367 (blue triangles), as well as the experimentally-derived values of $Q_{ht, glob}$ for the six key-points
 368 considered in this study (red circles). It can be noted that the values of the key-points are in trend.

369 The values of the squared correlation coefficient R^2 and of the root mean square error (RMSE)
 370 for the predicted vs. experimental values of $Q_{ht, glob}$ are also reported in the chart.



371
 372 **Figure 3 – Trend of the experimental values of the $Q_{ht, glob}$ parameter, as a function of the**
 373 **$q_{f, inj}/n$ quantity, for the engine map tests of ref [14] and for the key-points of the present**
 374 **study.**

375

376 It will be shown, in Section 5, that a correct estimation of this parameter is fundamental in order
377 to accurately predict the injected fuel quantities.

378 The estimation of the net energy of the charge, i.e., Q_{net} , allows the in-cylinder pressure to
379 be predicted in the interval between SOC and EOC, using a single zone approach, as follows:

380
$$dp = \left(\frac{\gamma - 1}{V} \right) \left(dQ_{net} - \frac{\gamma}{\gamma - 1} p dV \right) \quad (15)$$

381 The reconstruction of the complete in-cylinder pressure trace also includes the
382 compression and expansion phases, which are modeled by means of polytropic evolutions, and
383 the gas exchange phases, which are modeled as constant pressure evolutions (see [13-15]). In
384 particular, the following correlations were used to estimate the polytropic coefficients of the
385 compression and expansion phases:

386
$$m = 0.0011 q_{f, inj} (mm^3) + 1.30 \quad (16)$$

387
$$m' = -0.0016 q_{f, inj} (mm^3) + 1.38 \quad (17)$$

388

389 *3.1 Analysis of the cylinder-to-cylinder dispersion of the injectors*

390 Although only a single cylinder was instrumented for the pressure measurements, the
391 cylinder-to-cylinder dispersion of the injectors installed on the present engine was verified
392 indirectly on the basis of the analysis of the measured gas temperatures in the four exhaust
393 runners. In general, the temperatures of the exhaust gases outflowing from each cylinder depend
394 on combustion phasing (related to the injection phasing), on the air-to-fuel ratio (related to the
395 injected fuel quantity) and on heat transfer effects in the cylinders and in the runners. Outer
396 cylinders are in general characterized by higher heat transfer rates than inner ones.

397 Figure 4 reports the values of the exhaust gas temperatures in the four runners (Fig. 4a), as

well as the differences between the temperatures of the cyl1-cyl4 and cyl2-cyl3 exhaust runners (Fig. 4b).

It can be noted that the outer cylinders are characterized by systematically lower temperatures than the inner ones, due to a higher heat transfer rate. However, by comparing the temperatures of the outer cylinders (cyl1, cyl4), as well as those of the inner cylinders (cyl2, cyl3), it can be noted that the differences are small (i.e., of the order of 5-10°C)

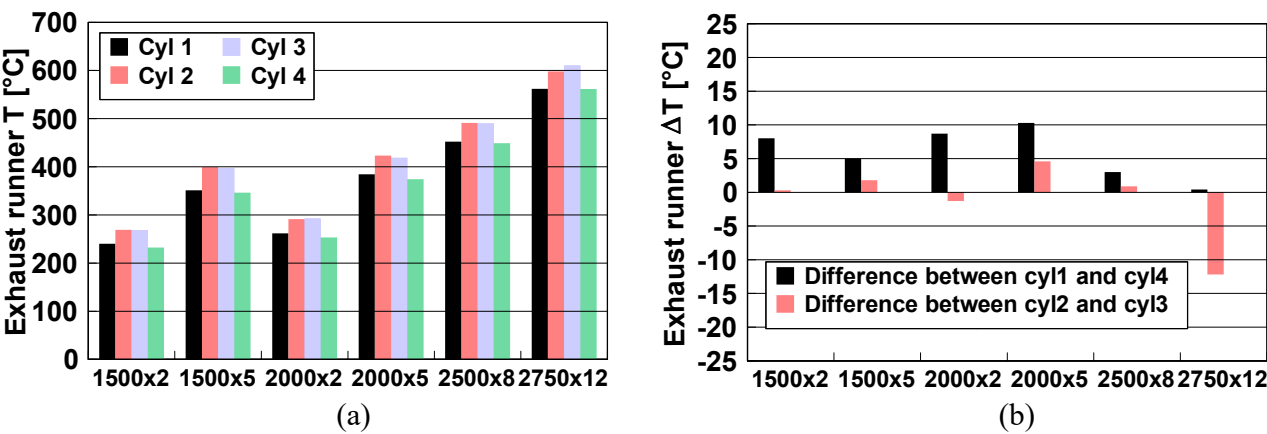


Figure 4 – Values of the gas temperatures in the exhaust runners of the four cylinders (a); differences between the temperatures of the gases in the cyl1 and cyl4 exhaust runners, as well as between the cyl2 and cyl3 ones (b).

This indirectly confirms that the behavior of the injectors installed in cyl1 and cyl4, as well as of those installed in cyl2 and cyl3, is very similar in terms of injection phasing and total injected quantity. In order to verify this, the combustion model was applied to the six key-points to test the impact of a deviation of ± 2 deg in the injection phasing of the main pulse, as well as of a deviation ± 1 mg in the injected quantity, on the predicted in-cylinder temperatures at EVO. The results are shown in Tab. 3.

Table 3 – Impact of variations in SOI_{main} and in the injected fuel mass on T_{EVO} , using the combustion model

Key-point	SOI _{main} +2deg	SOI _{main} -2deg	m _{f,inj} +1mg	m _{f,inj} -1mg
	ΔT_{EVO} [°C]	ΔT_{EVO} [°C]	ΔT_{EVO} [°C]	ΔT_{EVO} [°C]
1500x2	-4.6	5.3	36.8	-37.5
1500x5	-7.7	8.6	26.9	-27.0
2000x2	-6.0	6.5	37.0	-37.8
2000x5	-8.6	9.2	25.5	-26.2
2500x8	-10.5	11.3	18.1	-18.2
2750x12	-13.6	14.5	15.5	-15.6

It can be noted that the experimental differences in the exhaust gas temperatures shown in Fig. 4b correspond to a lower dispersion of the injected quantities than 1 mg/cyc for the same SOI_{main}, or to a lower dispersion of SOI_{main} than 2 deg for the same m_{f,inj}.

Moreover, in a recent research activity devoted to the refinement of the combustion model [17], each cylinder of a 1.6L GM engine has been instrumented with pressure transducers. It has been verified that the average cylinder-to-cylinder dispersion of IMEP was of the order of 0.6 bar (corresponding to a dispersion of the total injected quantity of about 0.5 mg/cyc), and that the average cylinder-to-cylinder dispersion of MFB50 was of the order of 0.5 deg. This confirms that the injector dispersion in modern diesel engines is very low.

4. ESTIMATION OF THE INJECTED MASS ON THE BASIS OF THE MEASURED IN-CYLINDER PRESSURE

The combustion model inversion procedure, which allows the injected fuel mass to be calculated as a model output, starting from the measured in-cylinder pressure time-histories, is reported hereafter.

A pilot-main injection strategy has been considered for the development of the method, which is however of general application. It has been assumed that the dwell-time between consecutive injections is not too short, so as to prevent overlapping of the heat release contributions that stem from the different injection pulses.

438 The dwell time threshold generally depends on the specific engine operating condition. In order
 439 to give some general indications, a dwell-time sweep was simulated using the combustion model for
 440 the six key-points. A threshold was identified for each key-point, under which a significant
 441 overlapping of heat release occurs between the pilot and main pulses. The thresholds are reported in
 442 Tab. 4.

443 **Table 4 – Estimated dwell-time threshold necessary to avoid significant overlapping between**
 444 **the pilot and main heat release**

	DT Threshold [μs]
1500x2	300
1500x5	400
2000x2	500
2000x5	500
2500x8	600
2750x12	600

445

446 Starting from Eq. (1), the $Q_{fuel}(t - \tau_j)$ term is made explicit as a function of $Q_{ch,j}$ for each injection
 447 pulse j, as follows:

448
$$Q_{fuel,j}(t - \tau_j) = Q_{ch,j}(t) + \frac{1}{K_j} \frac{dQ_{ch,j}}{dt}(t) \quad (18)$$

449 It is therefore necessary to obtain an experimental estimation of the $Q_{ch,j}$ curve for each
 450 injection pulse in order to evaluate the $Q_{fuel}(t - \tau_j)$ term. The estimation can be made as follows.

451 First, Eq. (11) is applied to evaluate the whole trend of the experimental charge net energy (i.e.,
 452 $Q_{net,exp}^{SOC}$) on the basis of the measured in-cylinder pressure.

453 The calculation is performed from SOC to EOC (a conventional EOC angle, e.g., 430°, can be
 454 assumed). The estimation of SOC is therefore necessary; this can be done according to the procedure
 455 illustrated in [21].

456 Once the estimation of $Q_{net,exp}^{SOC}$ has been carried out, the experimental trend of the released

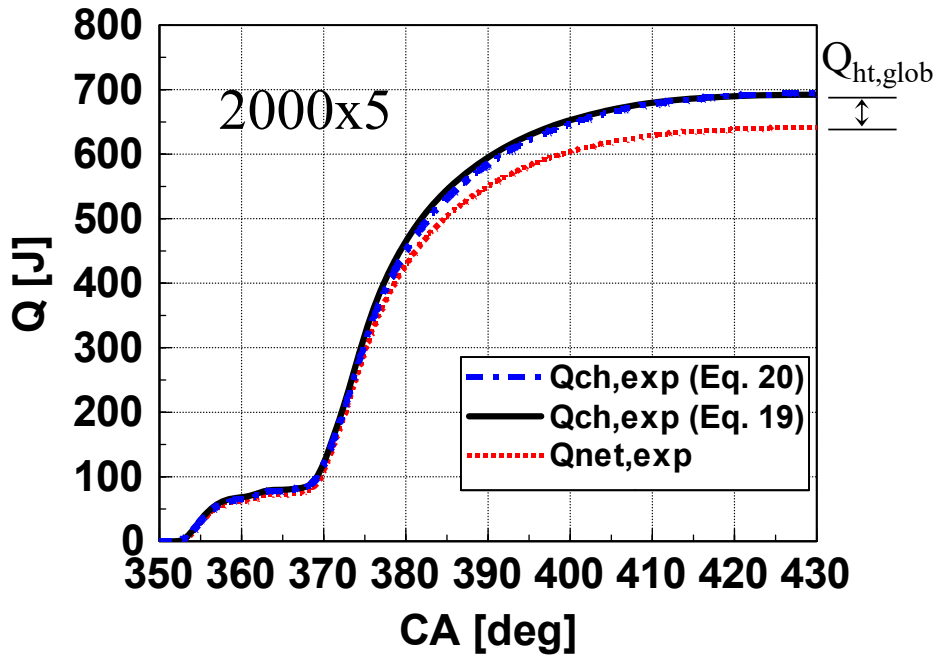
457 chemical energy (i.e., $Q_{ch,exp}^{SOC}$) is drawn by scaling the $Q_{net,exp}^{SOC}$ curve as follows:

$$458 \quad Q_{ch,exp}^{SOC} \cong Q_{net,exp}^{SOC} \frac{Q_{net,exp}^{SOC}(t_{EOC}) + Q_{ht,glob}}{Q_{net,exp}^{SOC}(t_{EOC})} \quad (19)$$

459 This is the inverse procedure to that used to estimate the Q_{net} curve on the basis of the Q_{ch}
 460 curve predicted by the combustion model (see Eq. (10)). The $Q_{ht,glob}$ parameter was introduced
 461 in Eq. (10) and represents the heat globally exchanged between the charge and the walls during
 462 combustion; it can be evaluated through Eq. (14), which was derived from experimental tests.

463 As an example, Fig. 5 reports, for the 1500x5 key-point, the experimental Q_{net} curve
 464 (dotted red line) and the experimental Q_{ch} curve obtained with Eq. (19) (black line). The $Q_{ht,glob}$
 465 parameter is also indicated in the figure. In addition, the experimental Q_{ch} curve obtained using
 466 a detailed heat transfer model is also reported with a blue chain line.

467



468 **Figure 5 – Trends of the experimental net and chemical energy release for the 2000x5**
 469 **key-point. The chemical energy release curves obtained from Eq. (19) and using a**
 470 **detailed heat transfer model (Eq. (20)) are reported.**
 471

The detailed heat transfer model is based on a convective formula [25]:

$$\dot{Q}_{ht} = hA(T - T_w) \quad (20)$$

where h is the convective heat transfer coefficient, A is the instantaneous heat transfer area, T is the instantaneous gas temperature and T_w is the wall temperature.

The convective heat transfer coefficient h [W/m²K] was modeled using the Woschni correlation [26]:

$$h[W / m^2 K] = c_0 B[m]^{-0.2} p[bar]^{0.8} T[K]^{-0.53} w[m / s]^{0.8} \quad (21)$$

$$w = \left[c_1 S_p[m / s] + c_2 \frac{V_d[m^3] T_r(IVC)}{p_r(IVC) V_r[m^3](IVC)} (p - p_m) \right] \quad (22)$$

where B is the bore diameter, S_p is the mean piston speed, V_d is the cylinder displacement, while T_r , p_r and V_r represent the in-cylinder temperature, pressure and volume at the moment of intake valve closure, respectively. c_0 was used as a calibration factor, while c_1 and c_2 were kept constant and equal to nominal values of 0.0039 and 2.31, respectively.

It can be observed, in Fig. 5, that the simplified procedure used to estimate Q_{ch} (i.e., Eq. (19)) leads to a good approximation of that obtained with the detailed heat transfer model (i.e., using Eq. (20)), even though a slight overestimation occurs for intermediate CA values between SOC and EOC. Similar trends were obtained for the other key-points, but the results are not reported here for the sake of brevity.

The approach based on the detailed heat transfer model requires the estimation of the instantaneous in-cylinder temperature, which is evaluated through the ideal gas law, using the measured in-cylinder pressure and the total trapped mass in the cylinder as input data. The latter quantity includes the contributions of air, EGR and residual gas.

This approach requires a higher computational time effort than the simplified approach (i.e., Eq.

495 (19)), and computational time is a critical parameter for control-oriented applications.

496 Once the $Q_{ch,exp}^{SOC}$ curve has been evaluated, it is necessary to split this curve into the single
497 contributions that stem from each injection pulse. As previously stated, it is assumed that
498 consecutive injections are scheduled using a moderately long dwell-time, in order to reduce the
499 overlapping of the heat release contributions that stem from the different pulses.

500 First, it is necessary to identify the SOC of each injection pulse. This can be done by
501 means of the methods reported in [21]. The overall SOC (i.e., that of the most advanced
502 injection pulse) is evaluated as the crank angle at which the first chemical energy fraction is
503 released. The SOC of the subsequent injection shots is detected by identifying the relative
504 minima of the HRR curve. This procedure is referred to as the “HRR local minima” (HLM)
505 method.

506 At this point, the experimental chemical energy release of the different injection pulses j
507 (i.e., $Q_{ch,j,exp}$, where j ranges from 1 to N , 1 indicates the most advanced pulse and N indicates
508 the most delayed one) can be calculated as follows. With reference to the most advanced pulse
509 (i.e., $j=1$):

$$\begin{aligned} 510 \quad Q_{ch,1,exp} &= Q_{ch,exp}^{SOC} \quad (t_{SOC} \leq t < t_{SOC,2}) \\ Q_{ch,1,exp} &= Q_{ch,exp}^{SOC}(t_{SOC,2}) \quad (t \geq t_{SOC,2}) \end{aligned} \quad (23)$$

511 where SOC is the overall start of combustion and SOC,2 is the SOC of the second
512 injection pulse.

513 The contribution of the chemical energy release of the subsequent pulses, excluding the
514 last one (i.e., $2 \leq j \leq N-1$), is instead calculated as follows:

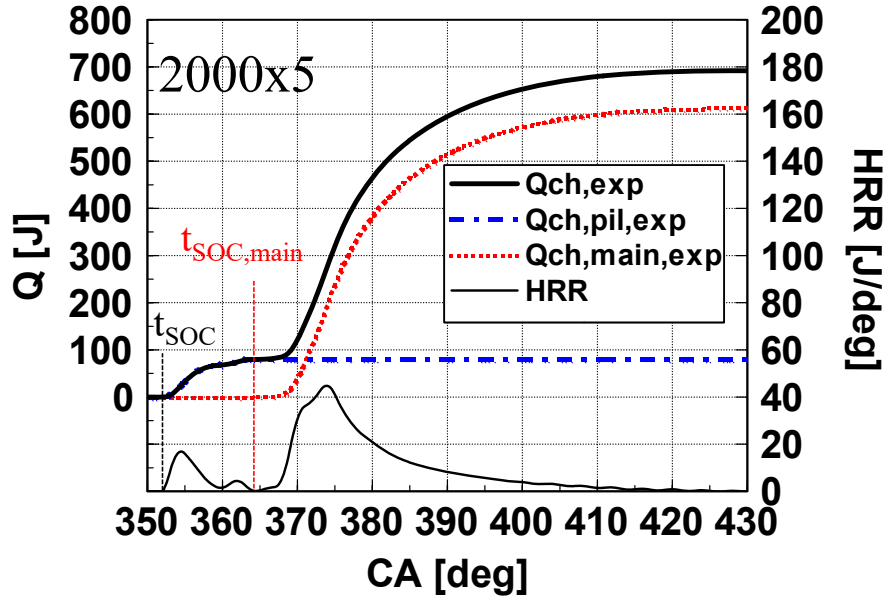
$$\begin{aligned} 515 \quad Q_{ch,j,exp} &= Q_{ch,exp}^{SOC} - Q_{ch,exp}^{SOC}(t_{SOC,j}) \quad (t_{SOC,j} \leq t < t_{SOC,j+1}) \\ Q_{ch,j,exp} &= Q_{ch,exp}^{SOC}(t_{SOC,j+1}) - Q_{ch,exp}^{SOC}(t_{SOC,j}) \quad (t \geq t_{SOC,j+1}) \end{aligned} \quad (24)$$

516 Finally, the contribution of the chemical energy release of the most delayed pulse (i.e.,

517 $j=N$), is derived as follows:

$$518 \quad Q_{ch,N,exp} = Q_{ch,exp}^{SOC} - Q_{ch,exp}^{SOC}(t_{SOC,N}) \quad (t_{SOC,N} \leq t \leq t_{EOC}) \quad (25)$$

519 The procedure is illustrated in Fig. 6 for the 2000x5 key-point featuring a pilot-main injection
 520 strategy.



521

522 **Figure 6 – Trends of the global experimental chemical energy release and contributions of**
 523 **the pilot and main injections evaluated with Eqs. (23-25) for the 2000x5 key-point. The trend**
 524 **of HRR is also reported.**

525

526 Figure 6 reports the overall experimental chemical energy curve (thick black line), as well as
 527 the contributions of the pilot (blue chain line) and main (pointed red line) pulses evaluated by
 528 means of Eqs. (23-25). The SOC instants evaluated with the above-mentioned procedures are also
 529 indicated, as is the HRR curve (thin black line).

530 The $Q_{fuel,j}$ term can now be estimated at time t through the following equation, which is derived
 531 from Eq. (18) taking the τ_j parameter into account:

$$532 \quad Q_{fuel,j}(t) = Q_{ch,j}(t + \tau_j) + \frac{1}{K_j} \frac{dQ_{ch,j}}{dt}(t + \tau_j) \quad (26)$$

533 The τ_j parameters are estimated by means of Equations (5-6); when input variables related
 534 to the injected quantities are used in the correlations to evaluate the model parameters (i.e., τ_j),
 535 the values derived from the injector maps can be used, to avoid iterative procedures; it was in
 536 fact verified that the resulting error in the evaluation of the ignition delay parameters is
 537 negligible.

538 The injected fuel mass curve of each injection pulse j can be estimated as follows:

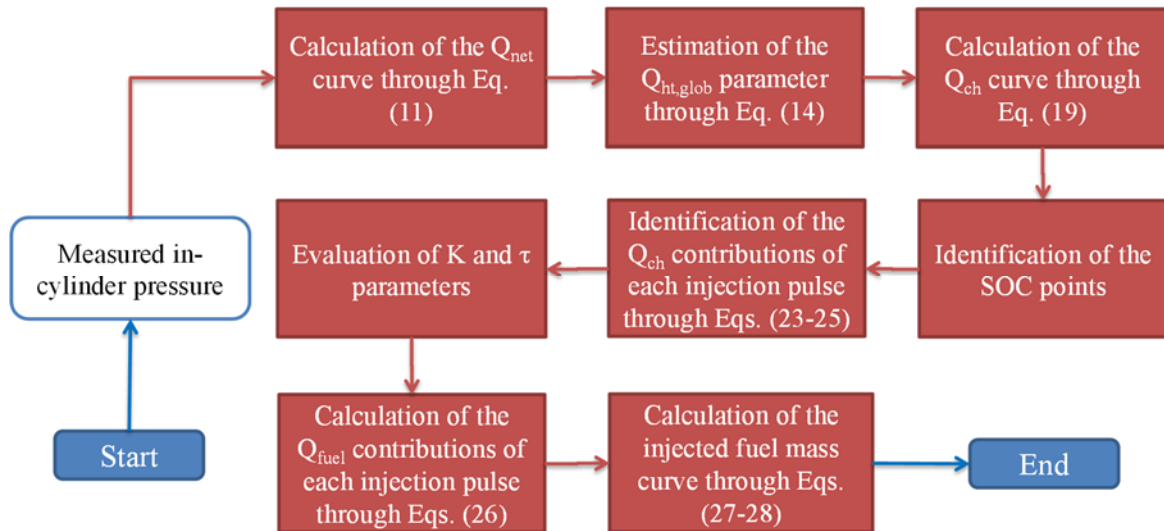
539
$$m_{f, inj, j} = \frac{Q_{fuel, j}}{H_L} \quad (27)$$

540 Finally, the total injected quantity of each pulse can be estimated evaluating the
 541 steady-state final value of the injected mass curve evaluated by means of Eq. (27).

542 The overall injected fuel mass curve, i.e., $m_{f, inj}$, is obtained by summing the contributions
 543 of all the injection pulses:

544
$$m_{f, inj} = \sum_{j=1}^N m_{f, inj, j} \quad (28)$$

545 Figure 7 shows a scheme that summarizes the proposed methodology.



546

547

Figure 7 – Scheme of the proposed methodology.

548 **5. RESULTS AND DISCUSSION**

549 The procedure explained in Section 4 was applied to the six key-points whose
550 specifications are reported in Tab. 2. In particular, a comparison was made between the injected
551 fuel mass estimated by means of the proposed method and those derived from the injector map;
552 moreover, a sensitivity analysis was carried out on the main model parameters, and the uncertainty
553 of the pressure-derived values of the injected fuel mass was evaluated.

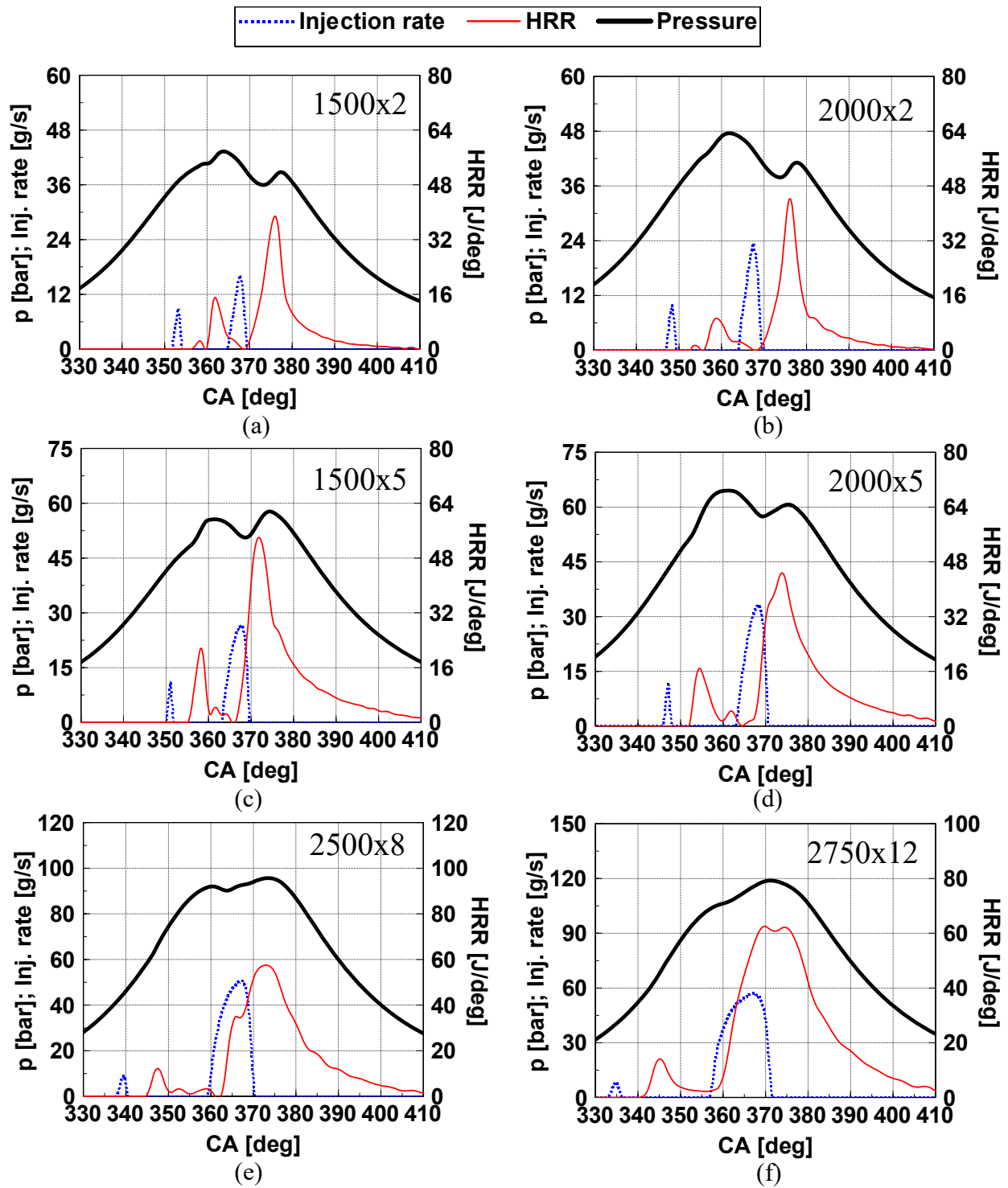


Figure 8 – Trends of the measured in-cylinder pressure, of the pressure-derived HRR and of the injection rate, for the six key-points.

Figure 8 reports the measured in-cylinder pressure trends (black lines), the HRR curves derived from the pressure traces using a single-zone model (thin red lines) and the injection

rate profiles (pointed blue lines) for the six key-points. The in-cylinder pressure traces shown in Fig. 8 were obtained as the average of 100 consecutive cycles, which were filtered using the TAF (Time-average filtering) procedure shown in [27]. This procedure is based on the following steps. First, the time average of the instantaneous pressure is evaluated in the discrete consecutive CA intervals into which the engine cycle is divided, and the resulting averaged pressure values, taken in the middle of the respective intervals, are interpolated through cubic spline fitting to obtain the original in-cylinder pressure curve.

It can be noted, in Fig. 8, that all the key-points feature a pilot-main injection strategy. Moreover, it can be observed, from the HRR traces, that the 1500x2, 2000x2 and 1500x5 key-points show dominant premixed combustion, while the remaining key-points show a premixed-mixing controlled combustion type. It can be noted that HRR premixed and mixing controlled combustion peaks for the latter key-points are of the same order of magnitude, due to the adoption of a pilot injection which leads to a reduction in the premixed combustion contribution. A single injection strategy would lead to much higher HRR peaks during the premixed combustion phase.

With reference to the model outcomes, Figure 9a reports, for the six key-points, the values of the pressure-derived total injected fuel mass, as well as the values obtained from the injector map and those derived from the fuel flow meter, while Fig. 9b reports the differences between the values obtained from the injector map/fuel meter and those derived from the measured pressure. Figure 9c, instead, reports the values of the pressure-derived pilot injected quantities as well as those derived from the injector map, while Fig. 9d shows the differences between the values obtained from the injector map and those derived from the measured in-cylinder pressure. Figures 6b-d also report the average uncertainty bands of the proposed method. The procedure to estimate the uncertainty is explained in Section 5.2.

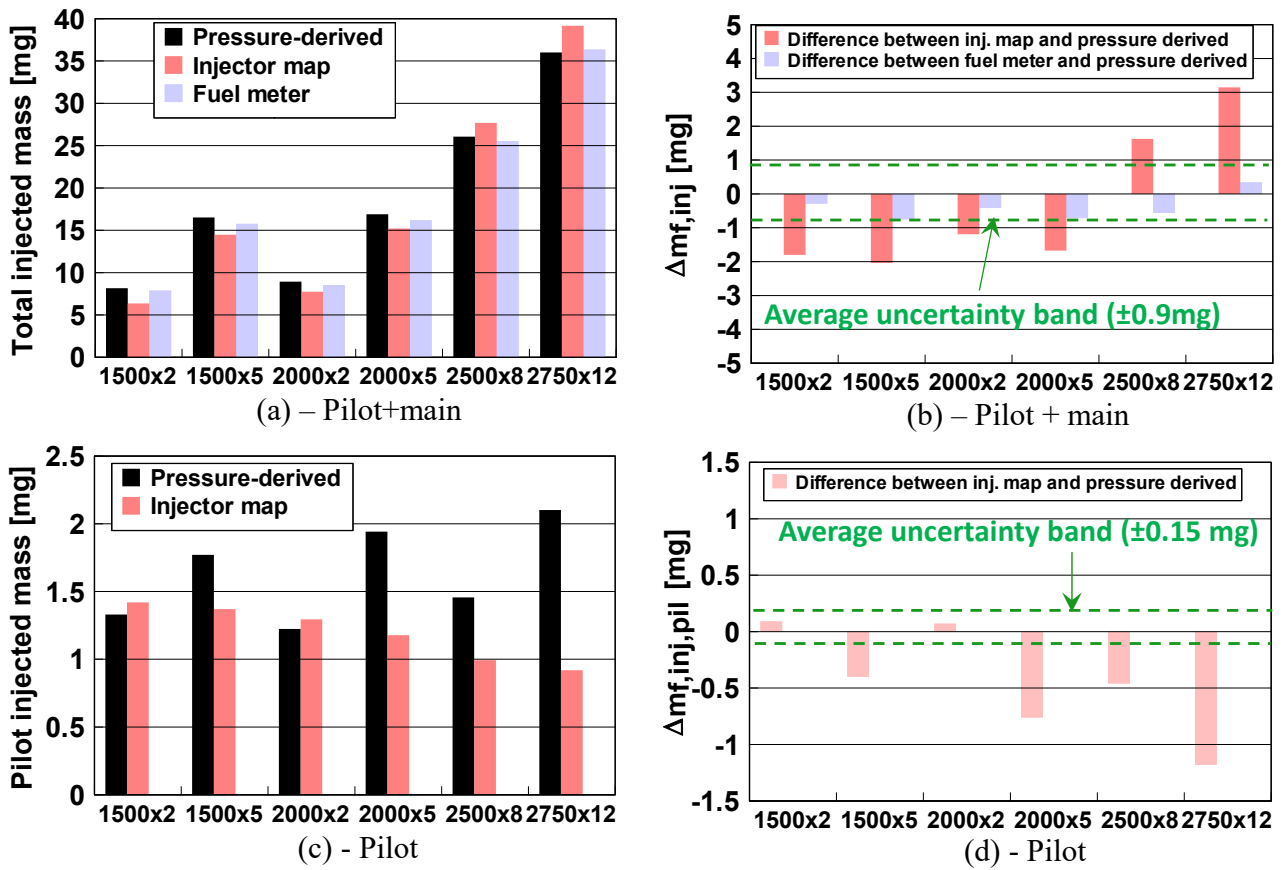


Figure 9 – Comparison between the total (a) and pilot (c) fuel injected quantities

derived from the in-cylinder pressure and those derived from the injector map (total, pilot) and fuel meter (total); difference between the injected quantities from the injector maps/fuel meter and those obtained from the in-cylinder pressure (b, d). The average uncertainty bands in the estimation of the pressure-derived injected quantities are also reported.

First, it can be noted that the average uncertainty in the evaluation of the injected mass of the pilot pulses is very small (Fig. 9d), as it is of the order of 0.15 mg. The average uncertainty in the evaluation of the total injected quantity is instead of the order of 0.9 mg, and it will be shown, in Section 5.2, that this value mainly depends on the uncertainty in the evaluation of the heat transfer parameter ($Q_{ht, glob}$) when Eq. (14) is used.

596

597 From the results reported in Fig. 9a-b, it can be observed that the pressure-derived total
598 injected quantities are comparable with those derived from the fuel meter, as the difference is below
599 the uncertainty band of the method. It can also be noted that the proposed method diagnoses several
600 deviations in the total injected quantities estimated by the injector map, (i.e., by the ECU): the
601 quantities of the medium-low load key-points (i.e., 1500x2-5, 2000x2-5) are underestimated, while
602 those of the medium-high load key-points (i.e., 2500x8, 2750x12) are overestimated. In particular,
603 the deviations of the ECU-derived total injected quantities are of the order of +3 mg for the
604 2750x12 key-point, of +1.7 mg for the 2500x8 key-point, of -1.5 mg for the 1500x2 and 2000x5
605 key-points and of -2 mg for the 2000x5 key-point. These deviations can be considered significant,
606 compared with the uncertainty of the method.

607 With reference to the pilot injected quantities, it can be observed that the method diagnoses
608 significant deviations in the quantities evaluated by means of the injector map at the 2750x12
609 key-point (-1.3 mg), at the 2000x5 (-0.8 mg) key-point, but also at the 1500x5 and 2500x8
610 operating conditions (about -0.4/-0.5 mg).

611

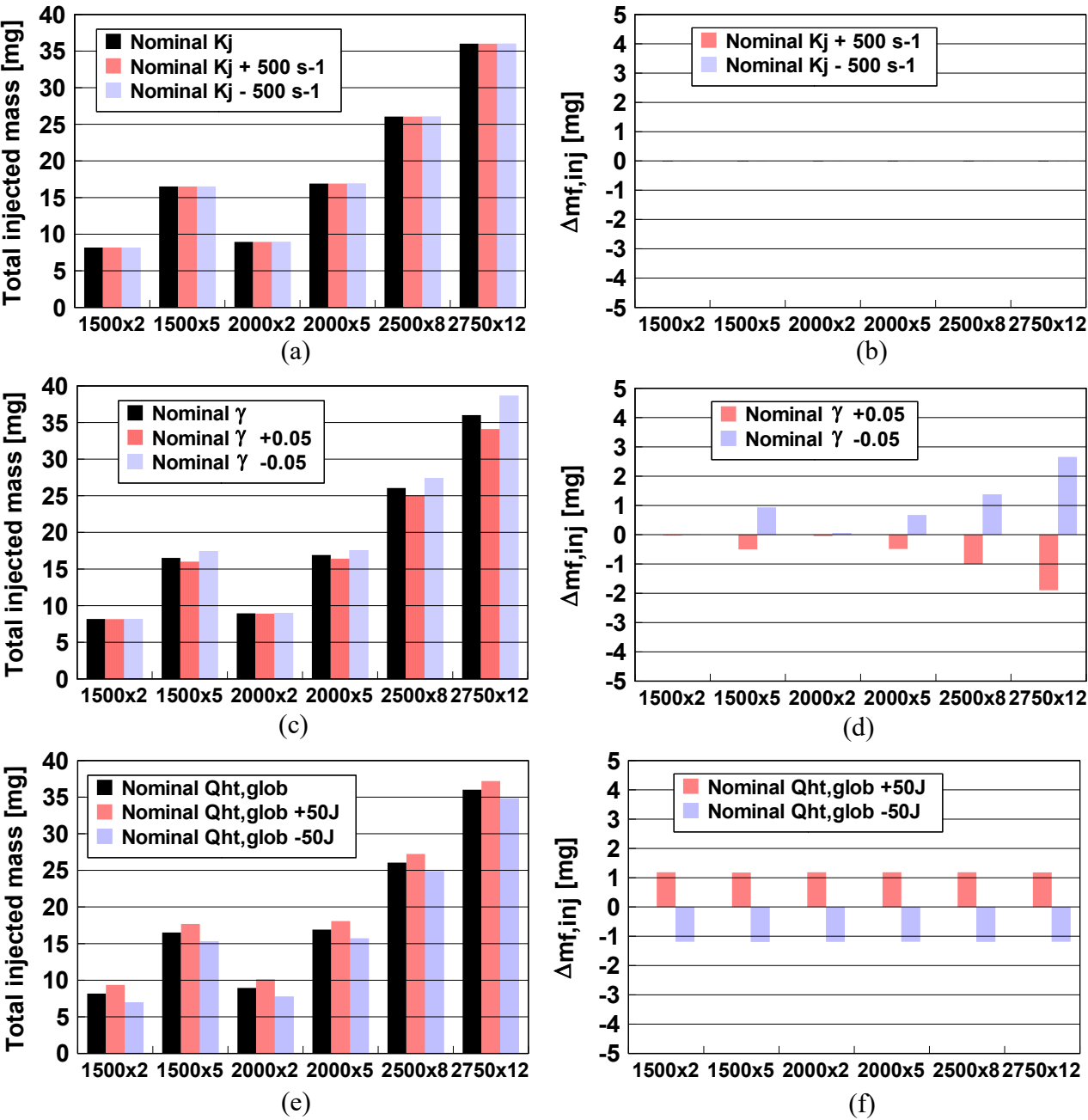
612 5.1 Sensitivity analysis

613 A sensitivity analysis was carried out in order to verify the effect of the main model parameters
614 on the pressure-derived injected quantities. The first three parameters that were considered in this
615 analysis are the values of the K_j coefficients of the combustion model (see Eq. (26)), the value of
616 the isentropic coefficient γ used in Eq. (11) to derive the experimental Q_{net} trace from the
617 in-cylinder pressure and the $Q_{ht, glob}$ parameter used in Eq. (19) to obtain the experimental Q_{ch} trace,
618 starting from the experimental Q_{net} trace; finally, the effect of horizontal and vertical shifts in the
619 in-cylinder pressure trace were also investigated.

620 Each parameter was varied separately, keeping the remaining ones unchanged. The analysis

621 was made for the all the key-points. Reasonable variation ranges were chosen for the
 622 parameters considered in the sensitivity analysis.

623



624
 625 **Figure 10 – Effect of a variation in the values of the K_j , γ and $Q_{ht,glob}$ parameters**
 626 **(with respect to the nominal values) on the estimated total injected mass (a, c, e). The**
 627 **differences are also reported (b, d, f).**

628

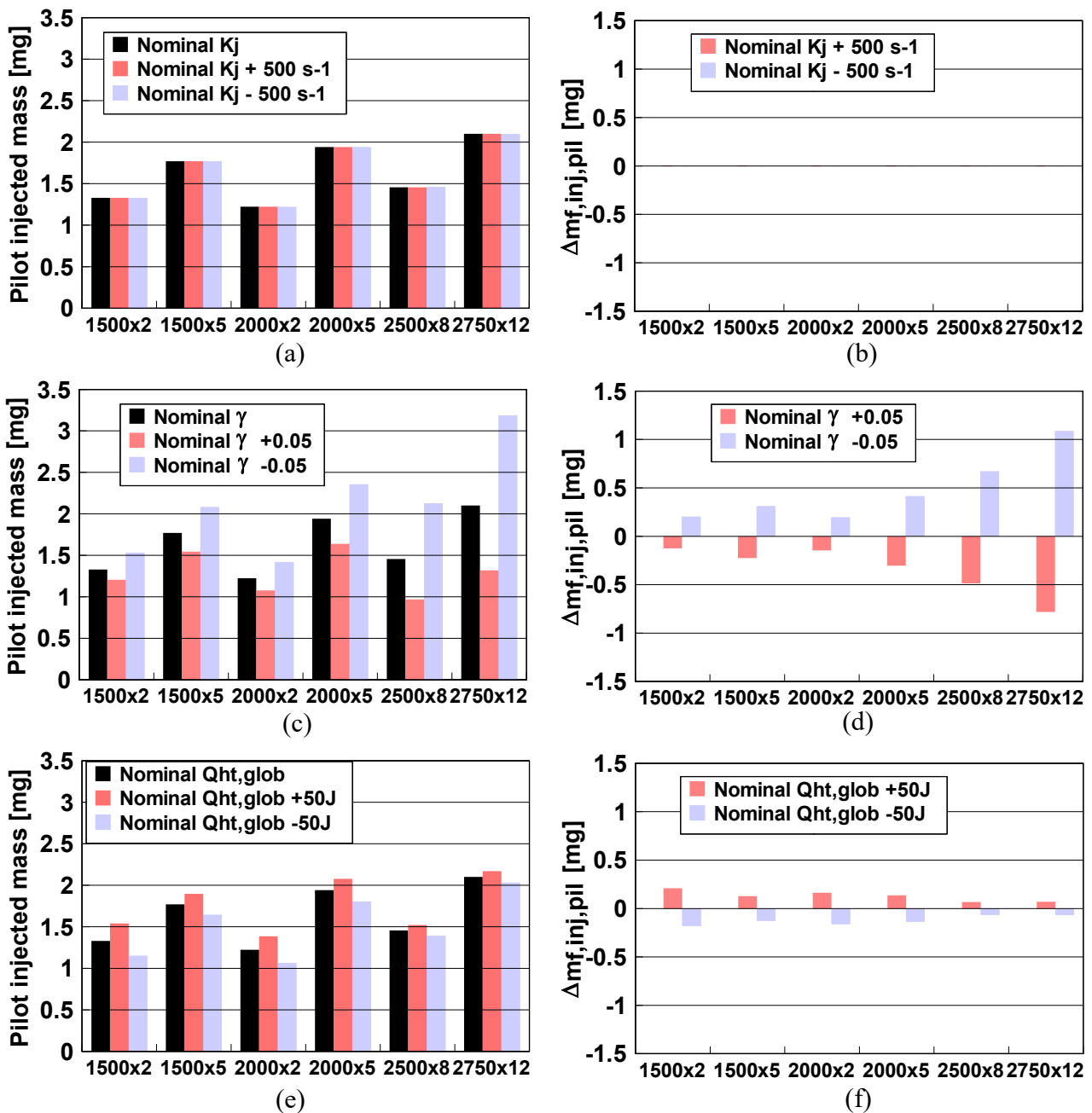


Figure 11 – Effect of a variation in the values of the K_j , γ and $Q_{ht, glob}$ parameters (with

respect to the nominal values) on the estimated pilot injected mass (a, c, e). The differences are also reported (b, d, f).

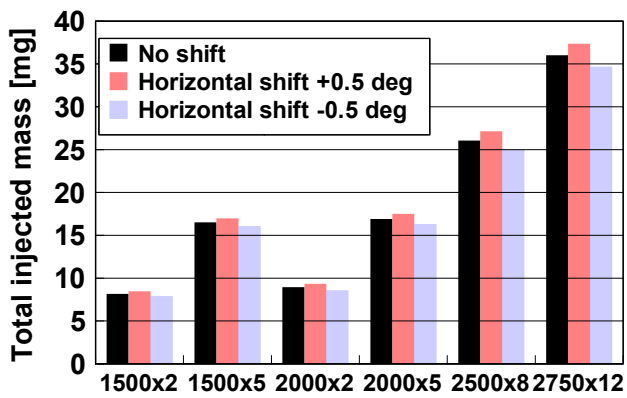
The results are shown in Figs. 10-13. Figures 10-11 report the effect of a variation in the values of the K_j (Figs. 10a, 11a), γ (Figs. 10c, 11c) and $Q_{ht, glob}$ (Figs. 10e, 11e) parameters, with respect to the nominal values, on the estimated total injected quantities (Fig. 10) and pilot injected quantities

637 (Fig. 11). The differences are also reported in Figs. 10b, 10d, 10f and 11b, 11d, 11f.

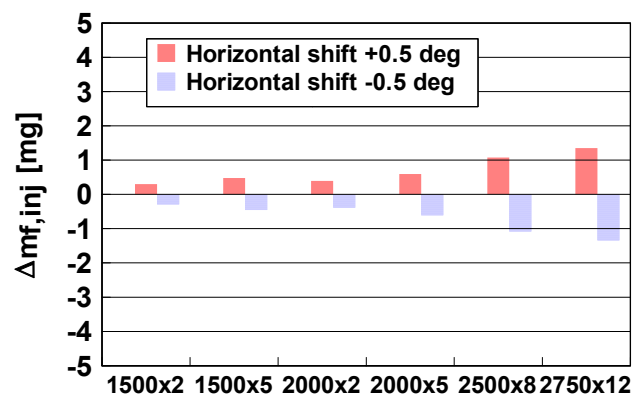
638 It can be noted that a variation in the values of the K_j parameter (Figs. 10a,b and 11a,b)
639 does not influence the pressure derived injected quantities to any great extent; a variation in the
640 values of the γ parameter has a remarkable effect on both the pressure-derived total injected
641 quantity (Figs. 10c, d) and on pilot injected quantity (Figs. 11c, d), and the effect increases with
642 the engine load. Finally, it is interesting to note that a variation in the value of $Q_{ht, glob}$ mainly
643 affects the diagnosed total injected quantities (the deviations are independent of the engine
644 load/speed), but has little influence on the diagnosed pilot injected quantities.

645 This analysis suggests that is important to accurately select the γ parameter to evaluate the
646 charge net energy Q_{net} (see Eq. (11)), as it can significantly affect the estimation of the total and
647 pilot injected quantities. Moreover, a good prediction of the heat transfer parameter $Q_{ht, glob}$ is
648 also required, as it directly affects the estimated total injected quantity. However, the impact of
649 this parameter on the estimated values of the pilot injected quantities can be considered
650 negligible, and this leads to low uncertainty, as will be shown in Section 5.2.

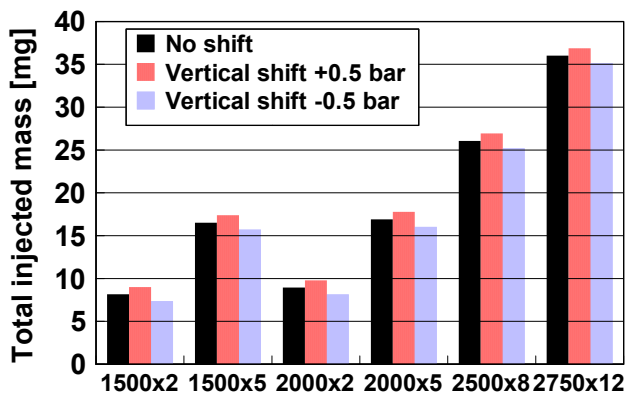
651 The estimation of the injected quantities could also be affected by an error in the measured
652 in-cylinder pressure trace, which is the main model input. Figures 12-13 report the effect of
653 horizontal and vertical shifts in the in-cylinder pressure trace on the estimated total injected
654 quantities (Fig. 12) and pilot injected quantities (Fig. 13).



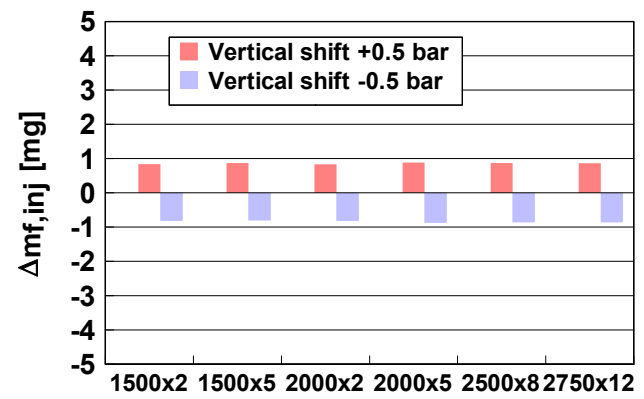
(a)



(b)



(c)



(d)

Figure 12 – Effect of a horizontal and vertical shift of the measured pressure on the estimated total injected mass (a, c). The differences are also reported (b, d).

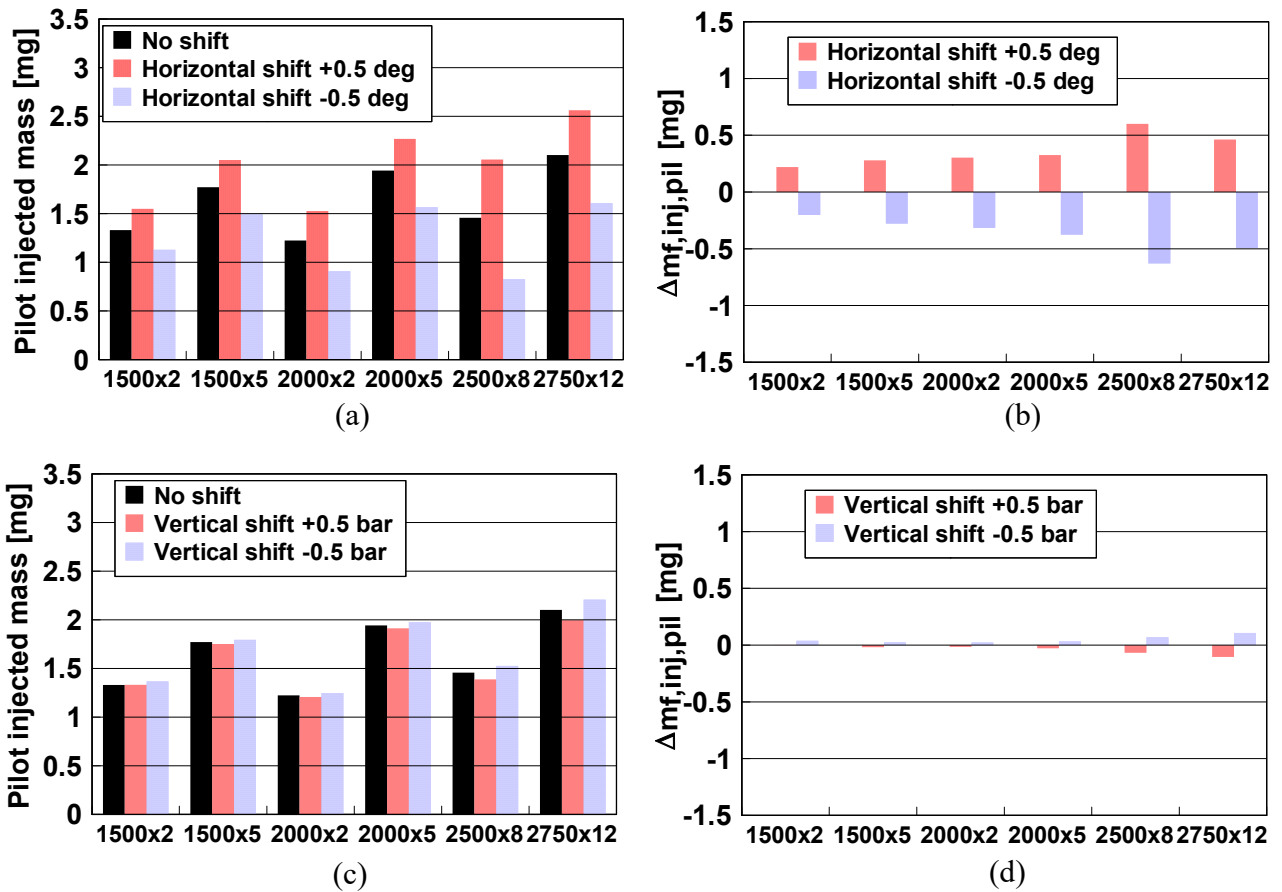


Figure 13 – Effect of a horizontal and vertical shift of the measured pressure on the estimated total injected mass (a, c). The differences are also reported (b, d).

It can be observed, in Fig. 12, that both horizontal and vertical shifts affect the pressure-derived total injected quantities to a great extent, and that the effect of a horizontal shift increases with engine load, while that of a vertical shift is somewhat constant.

With reference to the estimated pilot injected quantities (Fig. 13), it should be noted that a horizontal shift leads to significant deviations, which increase with the engine load, while a vertical shift has little influence.

As a result, attention should be paid to the correct pressure phasing, with respect to the crank angle, and to the correct in-cylinder pressure referencing. The latter may be realized comparing the values of the in-cylinder pressure around BDC with the values measured in the

672 intake manifold by means of an absolute pressure transducer.

673

674 5.2 Evaluation of the experimental uncertainty

675 The procedure applied for the evaluation of experimental uncertainties is based on the
676 recommended practices reported in [28] and hereafter summarized.

677 Given an output quantity y , which is dependent on N independent x_i variables, the associated
678 variance $u_c^2(y)$ is calculated through the following relation:

$$679 \quad u_c^2(y) = \sum_{i=1}^N \left(\frac{\partial y}{\partial x_i} \right)^2 u^2(x_i) = \sum_{i=1}^N c_i^2 u^2(x_i) \quad (29)$$

680 Equation (29) is consistent if the mutual effects between independent variables are neglected. c_i
681 is the “coefficient of sensitivity” of the output quantity y with respect to the i -th independent
682 variable x_i .

683 Once $u_c^2(y)$ has been evaluated, it is possible, by assuming a level of confidence (e.g., 95%)
684 and a correspondent coverage factor k (e.g., equal to 2), to evaluate the expanded combined
685 uncertainty of y , $U_c(y)$:

$$686 \quad U_c(y) = k \sqrt{u_c^2(y)} \quad (30)$$

687 If the independent variables x_i are the result of a measurement, the associated variance should
688 be estimated by taking into account the accuracy of the instrument declared in the calibration
689 certificate, the repeatability, the instrument resolution and the master uncertainty.

690 The procedure was used to estimate the uncertainty in the predicted values of the injected pilot
691 mass and of the total injected quantity for the six analyzed key-points.

692 The main parameters that could affect the estimation of the injected quantities were identified
693 and analyzed in Section 5.1. However, most of those parameters can be excluded from the
694 uncertainty calculation as they are not sources of error. First, it was shown that the K_j parameters

used in the heat release model do not affect the predicted injected quantities to any great extent (see Fig. 10a, 11a). The γ coefficient has remarkable influence on the predicted quantities (see Fig. 10b, 11b), and it should therefore be selected accurately. The correlation developed in [13], as a function of the RAFR parameter, was used in the present study (see Fig. 2 and Eq. (12)). The $Q_{ht, glob}$ parameter also has a significant effect on the estimated total injected quantities (see Fig. 10c) but has little influence on the estimated pilot injected quantities (see Fig. 11c).

Vertical and horizontal shifts in the in-cylinder pressure affect the estimation of Q_{net} and therefore of the pressure-derived injected quantities (see Fig. 11-12). However, if the in-cylinder pressure is referenced correctly (using, for example, an absolute pressure sensor in the intake manifold) and phased correctly (on the basis of the thermodynamic loss angle, see [29]), this error contribution can be excluded from the uncertainty calculation procedure.

The only parameters whose effect on the uncertainty of the method has been considered significant are therefore γ and $Q_{ht, glob}$. These parameters were evaluated, in this study, by means of the correlations expressed in Eq. (12) and Eq. (14), and shown in Fig 2 and Fig. 3, respectively. There are two main sources of error for each of the two parameters; the first one is related to the uncertainty in the input variables that are used in the correlations (i.e., RAFR in Eq. (12), $q_{f, inj}$ and n in Eq. (14)). The second source of error is related to the dispersion of the predicted values of γ and $Q_{ht, glob}$ (through Eq.(12) and Eq. (14), respectively) with respect to the experimental ones; this dispersion was quantified by means of the RMSE parameter, which is equal to 0.006 for the γ parameter and to 18 J for the $Q_{ht, glob}$ parameter, using the proposed correlations. The first source of error was evaluated for each parameter (γ , $Q_{ht, glob}$) by applying Eq. (29) to the analytical expression of γ and $Q_{ht, glob}$ expressed by Eqs. (12, 14), and assuming reasonable values for the variance of the RAFR, $q_{f, inj}$ and n parameters. The second source of error was evaluated on the basis of the RMSE values. However, it has been verified that the

719 first source of error is two orders of magnitude lower than the second one. Moreover, it has also
 720 been verified that the contribution of γ is low, compared to that of $Q_{ht, glob}$, but it increases with the
 721 engine load (as can also be seen in Figs. 10d, 11d).

722 Table 5 summarizes the expanded combined uncertainty of the pressure-derived pilot and total
 723 injected quantities. It can be noted that the uncertainty in the evaluation of the pilot quantity is very
 724 small, as its average is of the order of 0.15 mg. The average uncertainty in the evaluation of the total
 725 quantity is instead of the order of 0.9 mg, and is larger at higher engine loads. This uncertainty is
 726 mainly related to the dispersion of the predicted values of $Q_{ht, glob}$ by means of Eq. (14), and could be
 727 reduced if a more refined method were to be identified to estimate heat transfer.

728

729 **Table 5 – Evaluation of the expanded uncertainty U of the predicted injected quantities.**

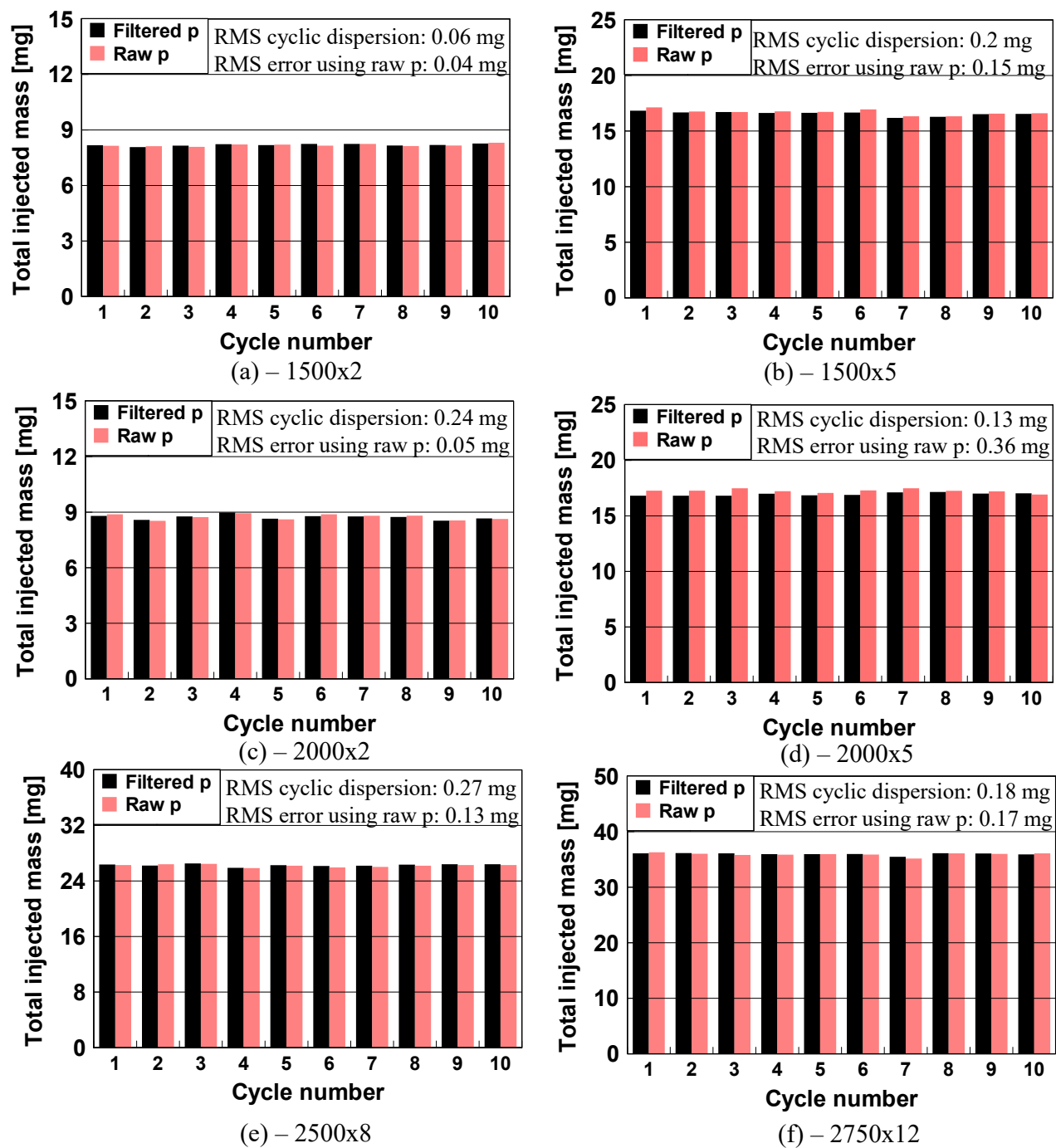
Key-point	Pilot	Pilot+main
	mg	mg
1500x2	0.15	0.85
1500x5	0.10	0.87
2000x2	0.15	0.85
2000x5	0.12	0.86
2500x8	0.15	0.90
2750x12	0.24	1.02

730

731 *5.3 Analysis of the cycle-by-cycle variations and considerations on the in-cylinder pressure quality*

732 The proposed methodology has also been tested on single, independent cycles in order to verify
 733 its capability of estimating cycle-by-cycle variations in the injected quantities. Moreover, the same
 734 analysis has been carried out using the acquired raw pressure, without TAF filtering, in order to
 735 verify the effect of signal noise on the outputs. This is an important aspect, as the use of the
 736 proposed method in commercial engines would require integrated pressure sensors, which are
 737 characterized by a higher signal noise than the Kistler sensor used in the present investigation.

738 Figures 14-15 report the estimated total and pilot injected quantities, respectively, for 10
 739 consecutive cycles using both filtered and raw pressure, for the six key-points.

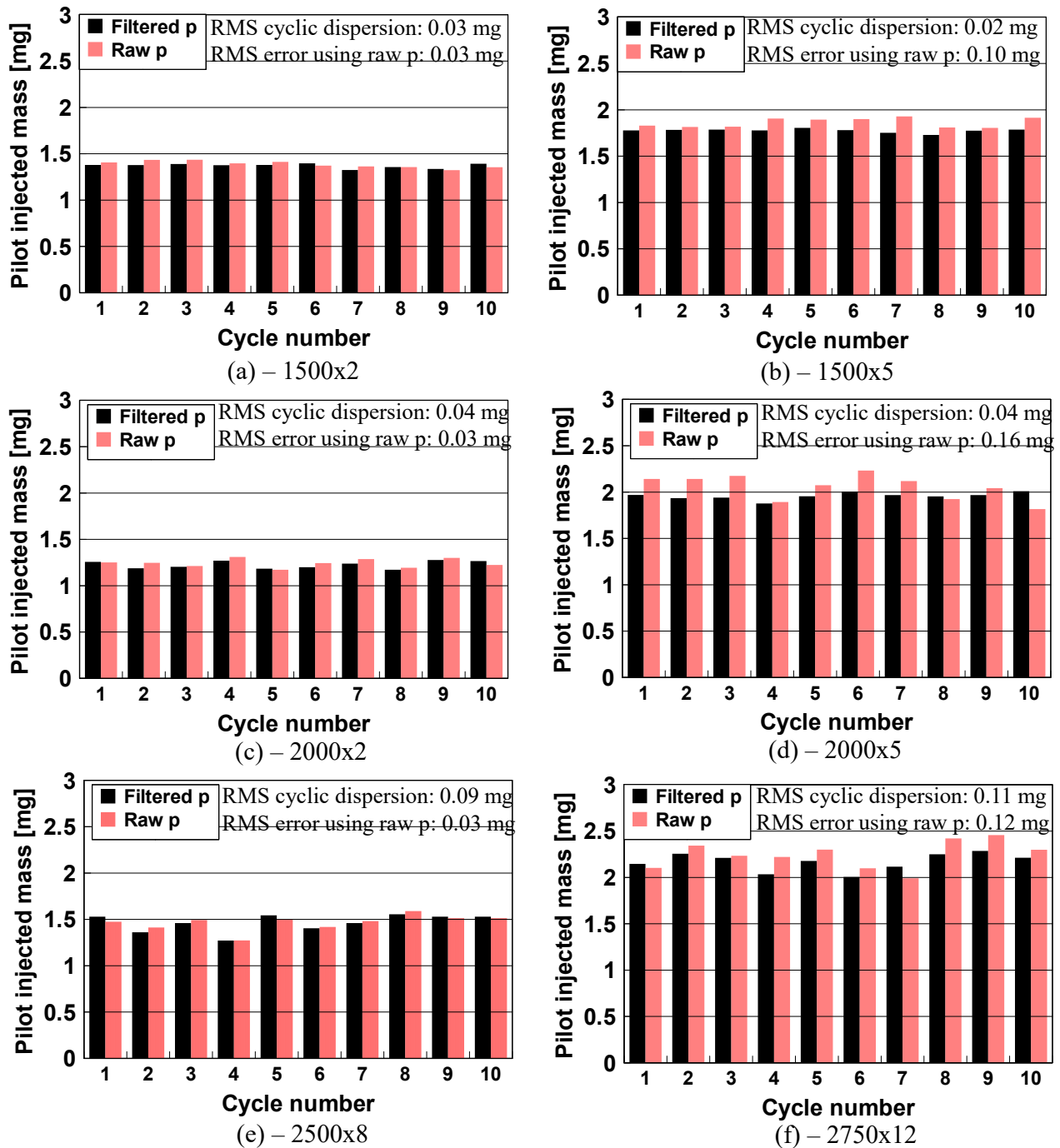


740
 741 **Figure 14 – Estimated total injected quantity for 10 consecutive cycles using both**
 742 **filtered and raw pressure. The RMS cyclic dispersion (calculated using the filtered**
 743 **pressure) and the RMS error of the raw pressure-derived quantities with respect to those**

744

derived from the filtered p are also reported.

745



746

747

Figure 15– Estimated pilot injected quantity for 10 consecutive cycles using both filtered

748

and raw pressure traces. The RMS cyclic dispersion (calculated using the filtered pressure)

749

and the RMS error of the raw pressure-derived quantities with respect to those derived from

the filtered pressure are also reported.

The RMS cyclic dispersion (calculated using the filtered pressure) and the RMS error of the injected quantities obtained from the raw pressure, with respect to those derived from the filtered pressure, are also reported in the graphs.

It can be noted that, in general, the cycle-by-cycle dispersion of both the pilot and total injected quantities is very low.

The method is also robust with respect to the use of a raw in-cylinder pressure signal. In this case, the errors depend on the specific engine operating conditions. The largest RMS errors occur at the 2750x12 and 2000x5 key-points, and are of the order of 0.36 and 0.17 mg/cyc, respectively, for the main pulse (see Fig. 14) and of the order of 0.12 and 0.16 mg/cycle, respectively, for the pilot pulses (see Fig. 15).

The use of a raw in-cylinder pressure is therefore suitable for estimating average injected quantities for all the operating conditions, while an accurate evaluation of cycle-by-cycle dispersion in general requires filtering of the pressure trace.

5.4 Analysis of the computational time

The computational time is basically expected to depend on the crank-angle step used for the in-cylinder pressure; this step should be chosen on the basis of a trade-off between the calculation time and the prediction accuracy.

An analysis has therefore been carried out in order to evaluate the impact of the crank-angle step on the computational time and on the prediction accuracy of the injected fuel quantities.

The elaboration was performed with the Labwindows CVI software, using a Pentium-D

774 PC.

775 The effect of the crank-angle step on the average computational time necessary to run a
776 single operating condition is reported in Tab. 6.

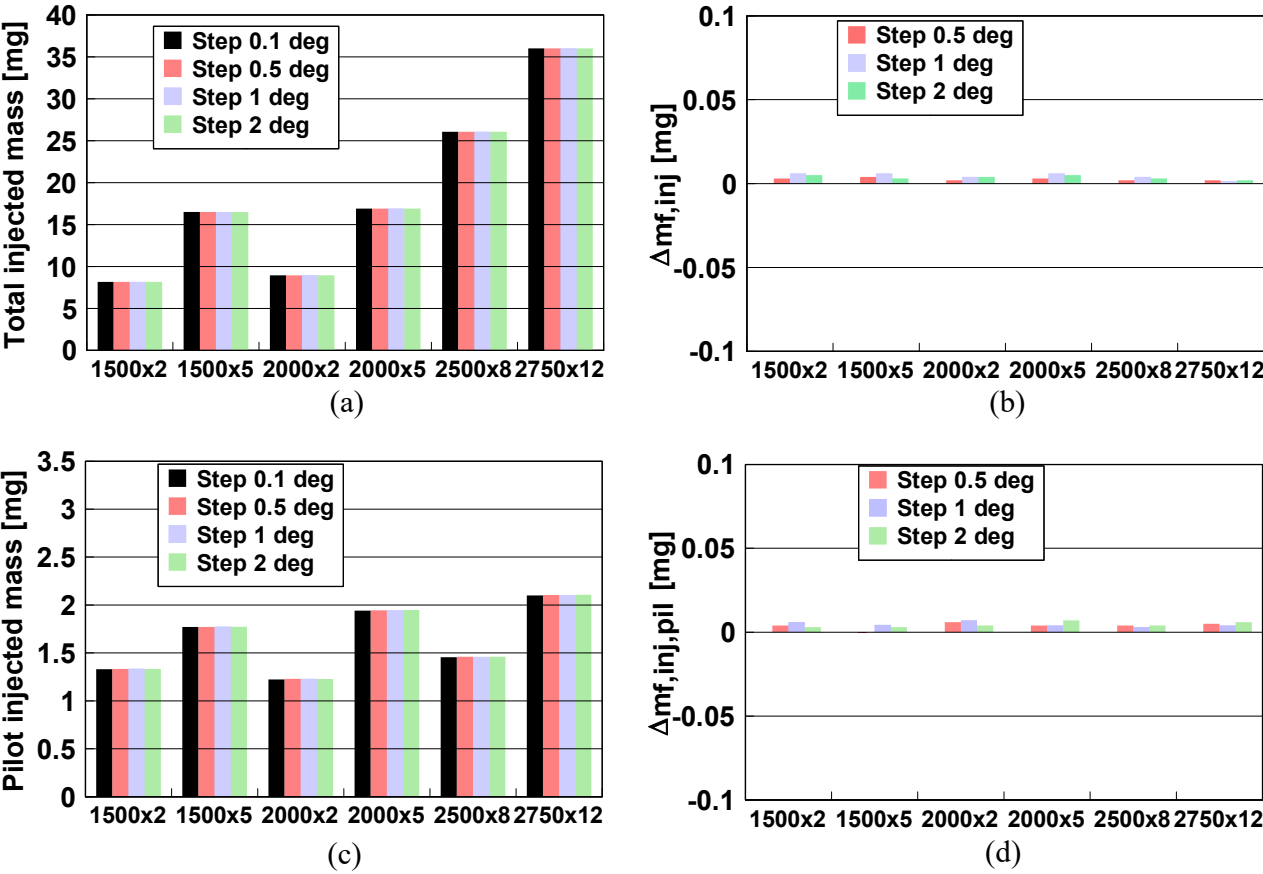
777

778 **Table 6 – Effect of the crank angle step on the computational time.**

Calculation step [deg]	0.1	0.5	1.0	2
Computational time: [ms]	3.4	0.9	0.6	0.3

779

780 Figure 16, instead, shows the effect of the crank angle step used for integration on the
781 estimated total and pilot injected quantities.



782

783 **Figure 16 – Effect of the crank angle step used for integration on the estimated total and**
784 **pilot injected quantities. The differences with respect to the case at 0.1 deg are also reported**

(b, d).

The analysis shows that the procedure is very robust with respect to the crank angle step used for integration. It should be specified that the net energy of the charge was calculated according to Eq. (11), using the trapezoidal rule for integration; it has been verified that this integration rule provides a nearly-independent trend of the net energy with respect to the crank angle step used for integration. The computational time that is required for a crank angle step of 2 deg is of the order of 0.3 ms. Therefore, the method can be considered suitable for control-oriented applications.

6. FUTURE WORK

In addition to the injected quantities, the proposed methodology also has the potential of estimating the injection rate curve on the basis of the measured in-cylinder pressure. This can be done by deriving Eq. (28) with respect to time.

An example is reported in Fig. 17 for the 1500x5 and 2000x5 key-points.

In particular, Fig. 17 reports a comparison between the injection rate profiles obtained with the measured in-cylinder pressure (black lines) and the experimental ones (dotted red lines).

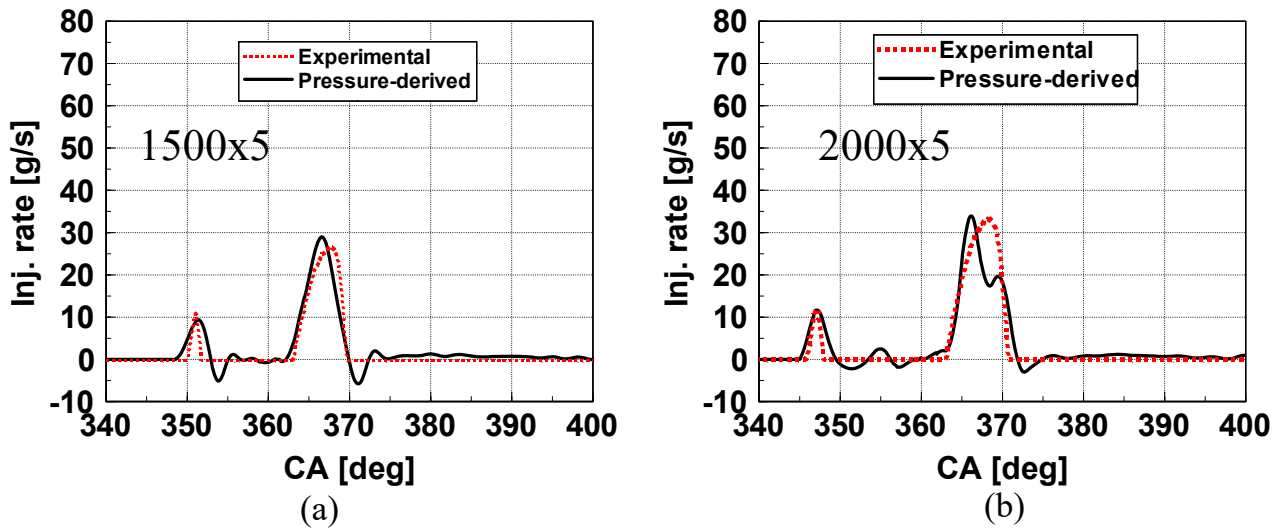


Figure 17 – Comparison between the pressure-derived injection rate profiles and the experimental ones for the 1500x5 and 2000x5 key-points.

It should be noted that the evaluation of the shape of the injection rate is quite good for the 1500x5 key-point, while it shows a double-peak characteristic for the main injection of the 2000x5 key-point. The accuracy of the prediction of the injection rate depends exclusively on the capability of the heat release model to correctly reproduce the HRR shape on the basis of the injection rate profile. It can therefore be observed, in Fig. 17, that the accumulated fuel mass approach (i.e., Eq. (1)) provides good results if the HRR shape is mainly of the premixed type, but is less accurate if the HRR shape is of the premixed-mixing controlled type (see Fig. 8). The result is that the injection rate shape derived from the in-cylinder pressure reflects the premixed-mixing controlled characteristics of the HRR (see Fig. 17b). A refinement in the prediction of the injection rate shape could be realized by refining the heat release model, using, for example, a crank-angle dependent value of the K_j parameters of Eq. (1). This investigation is currently ongoing.

Moreover, the applicability of the proposed method to highly premixed combustion modes, such as PCCI (Premixed Charge Compression Ignition) should also be verified.

824 7. CONCLUSION

825 A new methodology has been developed to estimate injected fuel quantities on the basis of the
826 measured in-cylinder pressure in multiple injection DI diesel engines.

827 The method is based on the inversion of a predictive combustion model that was
828 previously developed by the authors, and which is based on the accumulated fuel mass
829 approach.

830 A sensitivity analysis has been carried out in order to verify the effects of variations in the
831 main input parameters on the calculated injected quantities. It has been found that errors in the
832 estimation of the global heat transfer of $\pm 50\text{J}$ can lead to errors in the estimation of the total
833 injected quantities of about 1 mg/cyc , but the effect on the estimated pilot quantity error is
834 much smaller (below 0.2 mg/cyc). Moreover, errors in the estimation of the isentropic
835 coefficient γ of ± 0.05 lead to large errors for both the estimated total injected quantity (of up to
836 2 mg/cyc) and for the estimated pilot quantity (of up to 1 mg/cycle). It has also been verified
837 that horizontal shift errors on the in-cylinder pressure of $\pm 0.5\text{ deg}$ lead to errors in the
838 estimated total and pilot quantities of up to 1 mg/cyc and 0.5 mg/cyc , respectively, and vertical
839 shift errors on the in-cylinder pressure of $\pm 0.5\text{ bar}$ lead to errors in the estimated total quantity
840 of up to 0.8 mg/cyc , while the impact on the pilot quantity estimation error is negligible.

841 An uncertainty analysis has been carried out on the basis of the previous results. It has
842 been verified that the proposed method is robust when used to estimate the injected quantity of
843 the pilot pulses, as the average uncertainty is of the order of 0.15 mg . The average uncertainty
844 in the prediction of the total injected quantity is of the order of 0.9 mg , and depends mainly on
845 the accuracy of the evaluation of the heat transfer of the charge with the walls.

846 It has also been shown that the method is suitable for evaluating cycle-by-cycle variations
847 of the injected quantities, provided that the input pressure is filtered. However, it has been
848 verified that the use of the raw in-cylinder pressure allows the average injected quantities to be

849 estimated.

850 Finally, the approach is characterized by a very low computational time, that is, of the
851 order of 0.3 ms, when the elaboration is run on a PC and a crank angle integration step of 2 deg is
852 used, and is therefore suitable for control-oriented applications.

853

854 **ACKNOWLEDGMENTS**

855 GMPT-E is kindly acknowledged for the technical support in the activity.

856

857 **REFERENCES**

858 [1] Vanegas A, Won H, Felsch C, Gauding M. et al. Experimental Investigation of the Effect of
859 Multiple Injections on Pollutant Formation in a Common-Rail DI Diesel Engine. SAE Technical
860 Paper 2008-01-1191, 2008, doi:10.4271/2008-01-1191.

861 [2] Thurnheer T, Edenhauser D, Soltic P, Schreiber D, Kirchen P, Sankowski A. Experimental
862 investigation on different injection strategies in a heavy-duty diesel engine: Emissions and loss
863 analysis. Energ Convers Manage 2011; 52(1):457-467. doi: 10.1016/j.enconman.2010.06.074

864 [3] Catania AE, d'Ambrosio S, Ferrari A, Finesso R, Spessa E, Avolio G, Rampino V.
865 Experimental Analysis of Combustion Processes and Emissions in a 2.0L Multi-Cylinder Diesel
866 Engine Featuring a New Generation Piezo-Driven Injector. SAE Technical Paper 2009-24-0040,
867 2009, doi: 10.4271/2009-24-0040.

868 [4] Catania AE, Ferrari A., Manno M, Spessa E. Experimental Investigation of Dynamics
869 Effects on Multiple-Injection Common Rail System Performance. J. Eng. Gas Turbines Power
870 2008; 130(3): 032806-1-032806-13. doi: 10.1115/1.2835353.

871 [5] Catania AE, Ferrari A., Spessa E. Numerical-Experimental Study and Solutions to Reduce
872 the Dwell-Time Threshold for Fusion-Free Consecutive Injections in a Multijet Solenoid-Type CR
873 System. J Eng Gas Turbine Power 2008; 131(2): 022804-1-022804-14. doi: 10.1115/1.2938394.

- 874 [6] D'Ambrosio S, Ferrari A. Diesel Injector Coking: Optical-Chemical Analysis of
875 Deposits and Influence on Injected Flow-rate, Fuel Spray and Engine Performance. J Eng Gas
876 Turbine Power 2012; 134(6): 062801-1-062801-14. doi: 10.1115/1.4005991.
- 877 [7] Papagiannakis RG, Hountalas DT, Rakopoulos CD. Theoretical study of the effects of
878 pilot fuel quantity and its injection timing on the performance and emissions of a dual fuel
879 diesel engine. Energ Convers Manage 2007; 48(11):2951-2961. doi:
880 10.1016/j.enconman.2007.07.003
- 881 [8] Finesso R, Misul DA, Spessa E. Development and Validation of a Semiempirical
882 Model for the Estimation of Particulate Matter in Diesel Engines. Energ Convers Manage
883 2014; 84:374-389. doi: 10.1016/j.enconman.2014.04.053.
- 884 [9] Ponti F, Corti E, Serra G, De Cesare M. Common Rail Multi-Jet Diesel Engine
885 Combustion Model Development for Control Purposes. SAE Technical Paper 2007-01-0383,
886 2007. doi:10.4271/2007-01-0383.
- 887 [10] Ponti F, Ravaglioli V, Moro D, Serra G. MFB50 On-Board Evaluation Based on a
888 Zero-Dimensional ROHR Model. SAE Technical Paper 2011-01-1420, 2011.
889 doi:10.4271/2011-01-1420.
- 890 [11] Chmela FG, Orthaber GC. Rate of Heat Release Prediction for Direct Injection Diesel
891 Engines Based on Purely Mixing Controlled Combustion. SAE Technical Paper 1999-01-0186,
892 1999. doi:10.4271/1999-01-0186.
- 893 [12] Egnell R. A Simple Approach to Studying the Relation between Fuel Rate, Heat
894 Release Rate and NO Formation in Diesel Engines. SAE Technical Paper 1999-01-3548, 1999.
895 doi:10.4271/1999-01-3548.
- 896 [13] Catania AE, Finesso R, Spessa E. Predictive Zero-Dimensional Combustion Model for
897 DI Diesel Engine Feed-Forward Control. Energ Convers Manage 2011; 52(10):3159–3175, doi:
898 10.1016/j.enconman.2011.05.003.

- 899 [14] Catania AE, Finesso R, Spessa E, Catanese A, Landsmann G. Combustion Prediction by a
900 Low-Throughput Model in Modern Diesel Engines. SAE Int J Engines 2011; 4(1): 2106-2123. doi:
901 10.4271/2011-01-1410.
- 902 [15] Catania AE, Finesso R, Spessa E. Assessment of a Low-Throughput Predictive Model for
903 Indicated Cycle, Combustion Noise and NO_x Calculation in Diesel Engines in Steady-State and
904 Transient Operations. ICES2012-81094, Proceedings of the ASME 2012 Internal Combustion
905 Engine Division Spring Technical Conference, May 6-9, 2012, Torino, Italy. doi:
906 10.1115/ICES2012-81094.
- 907 [16] Arcidiacono M, Baratta M, Finesso R, Kheshtinejad H, Misul D, Spessa E, Yang Y. Use of
908 an Innovative Predictive Heat Release Model Combined to a 1D Fluid-Dynamic Model for the
909 Simulation of a Heavy Duty Diesel Engine. SAE Int. J. Engines 2013; 6(3):1566-1579.
910 doi:10.4271/2013-24-0012.
- 911 [17] Alfieri V, Conte G, Finesso R, Spessa E, Yang Y. HRR and MFB50 Estimation in a Euro 6
912 Diesel Engine by means of Control-Oriented Predictive Models. SAE Int. J. Engines
913 8(3):1055-1068, 2015, doi:10.4271/2015-01-0879.
- 914 [18] Guido C, Beatrice C, Di Iorio S., Napolitano P et al. Assessment of Closed-Loop
915 Combustion Control Capability for Biodiesel Blending Detection and Combustion Impact
916 Mitigation for an Euro5 Automotive Diesel Engine. SAE Technical Paper 2011-01-1193, 2011,
917 doi:10.4271/2011-01-1193.
- 918 [19] Schmid U, Seidel H. Study on an injection quantity sensor. I: Evaluation of the integration
919 procedure. Journal of Micromechatronics 2005; 3(1):15 – 32. doi: 10.1163/156856305323383892.
- 920 [20] Schmid U, Seidel H. Study on an injection quantity sensor. II: Evaluation of the sensing
921 element. Journal of Micromechatronics 2005; 3(1):33 – 50. doi: 10.1163/156856305323383900.
- 922 [21] Finesso R, Spessa E. Ignition delay prediction of multiple injections in diesel engines. Fuel
923 2014; 119(1):170-190. doi: 10.1016/j.fuel.2013.11.040.

924 [22] D'Ambrosio S, Finesso R, Spessa E. Calculation Of Mass Emissions, Oxygen Mass
 925 Fraction And Thermal Capacity Of The Inducted Charge In SI And Diesel Engines From Exhaust
 926 And Intake Gas Analysis. Fuel 2011; 90(1):152–166, doi:
 927 <http://dx.doi.org/10.1016/j.fuel.2010.08.025>.

928 [23] Catania AE, Finesso R, Spessa E. Real-Time Calculation of EGR Rate and Intake
 929 Charge Oxygen Concentration for Misfire Detection in Diesel Engines. SAE Technical Paper
 930 2011-24-0149, 2011. doi: 10.4271/2011-24-0149.

931 [24] Heywood JB. Internal Combustion Engine Fundamentals. McGraw-Hill, New York,
 932 1988.

933 [25] Finesso R, Spessa E. A Real Time Zero-Dimensional Diagnostic Model for the
 934 Calculation of In-Cylinder Temperatures, HRR and Nitrogen Oxides in Diesel Engines. Energ
 935 Convers Manage 2014; 79:498-510. doi: 10.1016/j.enconman.2013.12.045.

936 [26] Woschni G. A Universally Applicable Equation for the Instantaneous Heat Transfer
 937 Coefficient in the Internal Combustion Engine. SAE Technical Paper 670931, 1967, doi:
 938 10.4271/670931.

939 [27] Baratta M, d'Ambrosio S, Spessa E, Vassallo A. Cycle-Resolved Detection of
 940 Combustion Start in SI Engines by Means of Different In-Cylinder Pressure Data Reduction
 941 Techniques. ASME 2006 Internal Combustion Engine Division Spring Technical Conference
 942 (ICES2006), doi: 10.1115/ICES2006-1367.

943 [28] ISO/IEC GUIDE 98-3:2008(E).

944 [29] Rocco V. Dynamic T.D.C. and Thermodynamic Loss Angle Measurement in a D. I.
 945 Diesel Engine. SAE Technical Paper 851546, 1985, doi:10.4271/851546